


Research Paper

Resistive accretion flows around a Kerr black hole

M. Shaghaghian 

Department of Physics, Shiraz Branch, Islamic Azad University, Shiraz, Iran

Abstract

In this paper, we present the stationary axisymmetric configuration of a resistive magnetised thick accretion disc in the vicinity of external gravity and intrinsic dipolar magnetic field of a slowly rotating black hole. The plasma is described by the equations of fully general relativistic magnetohydrodynamics (MHD) along with the Ohm's law and in the absence of the effects of radiation fields. We try to solve these two-dimensional MHD equations analytically as much as possible. However, we sometimes inevitably refer to numerical methods as well. To fully understand the relativistic geometrically thick accretion disc structure, we consider all three components of the fluid velocity to be non-zero. This implies that the magnetofluid can flow in all three directions surrounding the central black hole. As we get radially closer to the hole, the fluid flows faster in all those directions. However, as we move towards the equator along the meridional direction, the radial inflow becomes stronger from both the speed and the mass accretion rate points of view. Nonetheless, the vertical (meridional) speed and the rotation of the plasma disc become slower in that direction. Due to the presence of pressure gradient forces, a sub-Keplerian angular momentum distribution throughout the thick disc is expected as well. To get a concise analytical form of the rate of accretion, we assume that the radial dependency of radial and meridional fluid velocities is the same. This simplifying assumption leads to radial independency of mass accretion rate. The motion of the accreting plasma produces an azimuthal current whose strength is specified based on the strength of the external dipolar magnetic field. This current generates a poloidal magnetic field in the disc which is continuous across the disc boundary surface due to the presence of the finite resistivity for the plasma. The gas in the disc is vertically supported not only by the gas pressure but also by the magnetic pressure.

Keywords: accretion – accretion discs – general relativistic magnetohydrodynamic – X-rays: binaries

(Received 17 July 2019; revised 3 November 2019; accepted 11 December 2019)

1. Introduction

Transforming gravitational energy into radiation in the most efficient possible form takes place in accretion onto black holes. It is certainly believed to be the primary power source behind the most luminous astrophysical systems that range from quasars and active galactic nuclei (AGNs) with very massive black holes to X-ray binaries with stellar-mass black holes. Due to the sufficiently high angular momentum content of the accreting matter, accretion does not happen as direct free fall onto a central star. Instead, it is expected to occur in the form of a disc. For formation of an accretion disc, it is necessary that the angular momentum is extracted from the inner to the outer regions of the disc. The transport mechanism of this angular momentum is complicated and not entirely clear (Lee & Ruiz 2002). Hence, regardless of the physics behind the cause responsible for this transport, Shakura & Sunyaev (1973) (hereafter SS73) suggested an enormously productive Ansatz about viscosity that is parameterised with an α -parameter. This parameterisation introduced by the standard model has been quite successful in interpreting the gross features of observational results.

It is generally believed that magnetic fields are ubiquitous in accretion discs and play a relevant role in their physical scenarios.

As a result, it is not unexpected that the magnetic fields are involved in a broad variety of dynamical processes of accretion discs. For instance, the magnetic stress may take the place of viscous stress of the standard model. Similar to the results of α -viscid disc of SS73, in a magnetised disc, about one-half of the released gravitational energy can dissipate through the Joule dissipation and the work done against the pressure force (Kaburaki 1986; 1987).

Knowing that the magnetic stress may drive disc turbulence and the outward transport of angular momentum, the theory of accretion disc is moving from the relatively simple parameterised, one-dimensional standard model of SS73 towards more realistic models. Considering the electrical conductivity for the plasma as a dissipative factor may be one of the most effective steps towards this aim. However, the underlying physics becomes more complex, especially when strong gravitational and external magnetic fields are also present. On account of this complexity, some authors intend to employ the limit of infinite conductivity, that is, the so-called ideal magnetohydrodynamics (MHD). In a no-resistive plasma, the magnetic lines of force freeze in and advect with the plasma. Furthermore, conservation of the magnetic flux passing through a moving surface in a no-resistive magnetofluid and no change in the topology of the magnetic field lines are of the other features of an ideal plasma. One important consequence of these properties is that the crossed magnetic field lines are not permitted to reconnect together in a perfectly conducting fluid (Eyink & Aluie 2006). Ideal MHD approximation applies widely in many astrophysical relevant situations including both theoretical models

Author for correspondence: M. Shaghaghian, E-mail: shaghaghian@iaushiraz.ac.ir

Cite this article: Shaghaghian M. (2020) Resistive accretion flows around a Kerr black hole. *Publications of the Astronomical Society of Australia* 37, e005, 1–18. <https://doi.org/10.1017/pasa.2019.50>

(Banerjee et al. 1997; Yuan & Narayan 2014) and numerical simulations (Koide, Shibata, & Kudoh 1999; De Villiers, Hawley, & Krolik 2003; McKinney & Gammie 2004).

Nevertheless, there are other physical circumstances in which this approximation no longer holds and it is important to include the effects of finite conductivity. For instance, in cold, dense plasmas around protostars (Fleming & Stone 2003) or dwarf nova systems (Gammie & Menou 1998), the ionisation fraction is so small. Furthermore, in the radiatively inefficient accretion flows (Foucart et al. 2016; 2017), despite the high temperature and fully ionised gas, the mean free path for coulomb interactions between charged particles is much larger than the typical size of the system. The accreting matter, in these cases, is probably expected to be nearly collisionless and its dynamical evolution may differ significantly from ideal MHD predictions as well. Inclusion of a finite resistivity as an angular momentum transport mechanism, particularly, is essential for a non-viscous disc to liberate the gravitational energy (Kaburaki 1986; 1987; Tripathy, Prasanna, & Das 1990; Banerjee et al. 1995; Kudoh & Kaburaki 1996; Koide 2010).

Accretion discs surrounding the black holes are among the most luminous objects in the universe. That is why they are the centre of special observational attention. They are also of considerable theoretical interest. To fully understand their structure and evolution, and to compare accurately the theoretical results with observational evidences, it is necessary to consider the influences of plasma interaction with all possible fields. These fields include a powerful relativistic gravitational field, a strong electromagnetic field, and an intense radiation field (Gammie & McKinney 2003). In this occasion, one encounters with a coupled set of partial differential equations that are time-dependent, multidimensional, and highly non-linear. Those equations may involve a large number of different physical quantities and free parameters. This, in turn, may be an obstacle on the way of analytical solutions and even numerical solutions of the equations due to the limitation of the ability of today's computers. Consequently, because of the level of complexity that the radiation field introduces, as the first feasible approximation, it seems reasonable that one ignores the radiation field and studies the problem in a non-radiating MHD mode.

The flows in the accretion discs may exhibit different morphologies from the viewpoint of their geometrical shape. They are generally divided into two distinct classes, thin discs and thick discs. Theory of thin accretion discs is well developed and has a fairly firm observational basis (SS73). However, thick accretion discs suffer mainly from the lack of an universally accepted model. Besides, their relevant observations are still rare and indirect. Therefore, there are still many theoretical uncertainties about their nature and structure. Nevertheless, observational and theoretical studies of thick accretion discs are of special astrophysical importance. Since willy-nilly, such structures have been suggested as models of quasars, AGNs, some X-ray binaries and are probably present in the central engine of gamma-ray bursts (Abramowicz, Karas, & Lanza 1998; Font & Daigne 2002).

Low-mass X-ray binaries are excellent laboratories for experimenting accretion physics because they are much closer than the AGNs and are therefore somewhat easier to observe (Higginbottom 2018). When the central compact object is a black hole, it is usual that the dynamics obey the general relativistic. Accordingly, we pursue the fully general relativistic magnetofluids around a typical black hole in a low-mass X-ray binary system such as Cygnus X-1. In this context, we are motivated to put aside the ideal MHD approximation and investigate the resistive accretion

disc structure without invoking the thin disc approximation in the absence of the effects of radiation field.

Standard thin disc theory of SS73 is characterised by the equilibrium of centrifugal and gravitational forces in the radial direction. It leads to the Keplerian rotation law throughout the disc. Whereas there is no net gas flow in the vertical direction, momentum conservation equation in that direction reduces to the hydrostatic equilibrium equation. Once the thin disc approximation is laid aside, the vertical thickness becomes comparable with its radial extension. The pressure gradient forces provide an essential support in the radial as well as meridional direction. At this moment, gravity cannot be balanced by centrifugal forces any more. The rotation law is no longer Keplerian and the vertical hydrostatic equilibrium is abandoned. Another key characteristic of SS73 theory is its subcritical luminosity. It means that the maximum possible luminosity of the standard geometrically thin discs is the Eddington luminosity. That is, the luminosity in which the inward gravity on accreting fluid is precisely counterbalanced by the outward radiation pressure gradient force of photons. Evidently, if the disc's luminosity exceeds the Eddington value, then some matter will be blown off by the pressure of the supercritical radiation flux in the form of a wind or a collimated bipolar jet (Okuda 2002; Takeuchi, Ohsuga, & Mineshige 2010; Takahashi & Ohsuga 2015).

As a result, we are interested in relativistic accretion tori around a slowly rotating black hole in the sub-Eddington regime and non-radiating mode, considering all three components of flow velocity to be non-zero. Particularly in what concerns the relativistic geometrically thick accretion discs, most of the previous works are mainly devoted to equilibrium toroidal configurations. That is, the flow restricted to the azimuthal component only, with assumption that the radial and meridional components are negligible in comparison with the azimuthal one (Banerjee et al. 1997; Kovar et al. 2011; Trova et al. 2018). Similar to our idea, both in Newtonian regime (Tripathy, Prasanna, & Das 1990) and in relativistic regime for a non-rotating Schwarzschild black hole without the vertical component for the magnetofluid velocity (Shaghaghian 2016), already have been done. It is known that almost all of the celestial bodies have a non-zero spin, and thus, the Schwarzschild geometry does not tell the whole story. Thus, we extend this idea to the case of slowly rotating black hole and let the magnetofluid flows in all three directions.

The structure of this paper is organised as detailed below: we begin in the next section, with a presentation of the theoretical framework used to construct our desired model and to describe the background geometry and the external magnetic field. Also, we depict our disc scheme in this section. The general formalism of the problem is discussed in Section 3. It includes the basic equations governing the relativistic magnetised flow accreted from the plasma around a slowly rotating black hole in the form of a thick torus, as well as their self-consistent solutions along with the physical simplifications of the problem. Our main conclusions are summarised in Section 4.

2. The model

2.1. Spacetime

To investigate the relativistic accretion flows around a rotating black hole, we follow closely the Boyer–Lindquist spherical coordinates t, r, θ, φ with the origin fixed on the central black hole and the z -axis chosen as the axis of rotation. Moreover, the self-gravity

of the surrounding magnetofluid is considered to be negligible in comparison with the gravitation of the central object. Thus, the background geometry supporting the disc is entirely determined by the central body and is defined by Kerr metric

$$ds^2 = \left(1 - \frac{2r}{\Sigma}\right) dt^2 + \frac{4ar \sin^2 \theta}{\Sigma} dt d\varphi - \frac{\Sigma}{\Delta} dr^2, -\Sigma d\theta^2 - \frac{A \sin^2 \theta}{\Sigma} d\varphi^2, \tag{1}$$

where $\Delta = r^2 - 2r + a^2$, $\Sigma = r^2 + a^2 \cos^2 \theta$ and $A = (r^2 + a^2)^2 - \Delta a^2 \sin^2 \theta$. Throughout this paper, we adopt geometric units $M = G = c = 1$ as our basic scalings. Here, M , G , and c are the central black hole mass, the universal gravitational constant, and the speed of light, respectively. This implies $M = 10 M_\odot$ as a unit of mass, and also $m = \frac{GM}{c^2}$ and $t_0 = \frac{GM}{c^3}$ as the units of length and time, respectively. Furthermore, rotation of the black hole is parameterised by Kerr parameter a , as the total angular momentum per unit mass of the black hole (i.e. $a = \frac{J}{Mc}$). Indeed, a may be measured in unit of length through a dimensionless spin parameter α as $a = \alpha m$.

It is widely believed that black holes are probably maximally rotating (Koide 2010; Tchekhovskoy, Narayan, & McKinney 2011). However, even on a test particle level, solutions using the fully rotating black hole seem to be an extremely formidable task. To avoid this complexity, astrophysicists in analytic modelling tend to approximate the black hole to be non-rotating characterised by the Schwarzschild metric or to be slowly rotating characterised by the linearised Kerr metric. However, in simulation community, this approximation is not popular (Porth et al. 2019). Note that the slowly rotating regime which is an acceptable approximation in the analytic astrophysics community means that one considers up to linear order of the Kerr-rotating parameter in the metric functions, governing equations and physical quantities (Prasanna 1989; Rezzolla 2001; Shaghaghian 2011; Harko, Kovacs, & Lobo 2011). Therefore, the linearised form of metric (1) is summarised as

$$ds^2 = \left(1 - \frac{2}{r}\right) dt^2 - \left(1 - \frac{2}{r}\right)^{-1} dr^2 - r^2 (d\theta^2 + \sin^2 \theta d\varphi^2) + \frac{4a}{r} \sin^2 \theta dt d\varphi. \tag{2}$$

2.1.1. Locally non-rotating frame

Once the background spacetime geometry rotates, it is necessary to establish an inertial frame in which the frame-dragging effects of the hole’s spin are vanished. A set of local observers as zero angular momentum observers are introduced (Yokosawa & Inui 2005). They rotate with the angular velocity ω and live at constant r and θ , but at $\varphi = \omega t + \text{const}$. This frame that becomes inertial at a far distance from the hole is so-called locally non-rotating frame (LNRF). Applying slowly rotating black hole approximation, the explicit transformations between the LNRF and the Boyer–Lindquist frame given by Bardeen, Press, & Teukolsky (1972) are simplified as

$$\lambda_i^{(a)} = \begin{bmatrix} \left(1 - \frac{2}{r}\right)^{1/2} & 0 & 0 & 0 \\ 0 & \left(1 - \frac{2}{r}\right)^{-1/2} & 0 & 0 \\ 0 & 0 & r & 0 \\ -\frac{2a}{r^2} \sin \theta & 0 & 0 & r \sin \theta \end{bmatrix},$$

and

$$\lambda_{(a)}^i = \begin{bmatrix} \left(1 - \frac{2}{r}\right)^{-1/2} & 0 & 0 & 0 \\ 0 & \left(1 - \frac{2}{r}\right)^{1/2} & 0 & 0 \\ 0 & 0 & \frac{1}{r} & 0 \\ \frac{2a}{r^3} \left(1 - \frac{2}{r}\right)^{-1/2} & 0 & 0 & \frac{1}{r \sin \theta} \end{bmatrix},$$

satisfying

$$\lambda_{(a)}^i \lambda_{(b)}^j g_{ij} = \eta_{(a)(b)},$$

where g_{ij} and $\eta_{(a)(b)}$ are the metric and Minkowski tensors, respectively. Noting here that parentheses around the indices represent the components in LNRF. The physical variables are transformed in this frame as follows:

$$F_{(\alpha)(\beta)} = \lambda_{(a)}^i \lambda_{(b)}^j F_{ij}, J^{(\alpha)} = \lambda_i^{(\alpha)} J^i, V^\alpha = \frac{\lambda_{(\beta)}^\alpha V^{(\beta)} + \lambda_{(0)}^\alpha}{\lambda_{(\beta)}^0 V^{(\beta)} + \lambda_{(0)}^0},$$

where F and J are the electromagnetic field tensor and the 4-vector electric current density, respectively. Moreover, V^α is the spatial 3-velocity and is defined through the relation $u^\alpha = u^0 V^\alpha$ to the 4-velocity u . We follow the (+, −, −, −) signature convention and the 4-velocity normalisation condition as $u^i u_i = 1$. It gives the following general definition for the zeroth component of 4-velocity u

$$u^0 = (g_{00} + 2g_{0\alpha} V^\alpha + g_{\alpha\beta} V^\alpha V^\beta)^{-1/2},$$

which in linearised Kerr metric [equation (2)] is simplified as

$$u^0 = \left(1 - \frac{2}{r}\right)^{-1/2} (1 - V^2)^{-1/2}. \tag{3}$$

The total fluid velocity V is related to its components as

$$V^2 = [V^{(r)}]^2 + [V^{(\theta)}]^2 + [V^{(\varphi)}]^2,$$

wherein

$$V^{(r)} = \left(1 - \frac{2}{r}\right)^{-1} V^r, V^{(\theta)} = r \left(1 - \frac{2}{r}\right)^{-1/2} V^\theta, V^{(\varphi)} = r \sin \theta \left(1 - \frac{2}{r}\right)^{-1/2} \left(V^\varphi - \frac{2a}{r^3}\right).$$

Furthermore, the components of field tensor and current density tensor are transformed as

$$B_r = r^2 \sin \theta B_{(r)}, B_\theta = r \sin \theta \left(1 - \frac{2}{r}\right)^{-1/2} B_{(\theta)},$$

$$\begin{aligned}
 B_\varphi &= r \left(1 - \frac{2}{r}\right)^{-1/2} B_{(\varphi)}, \\
 E_r &= \frac{2a}{r^2} \sin \theta \left(1 - \frac{2}{r}\right)^{-1/2} B_{(\theta)} + E_{(r)}, \\
 E_\theta &= -\frac{2a}{r} \sin \theta B_{(r)} + r \left(1 - \frac{2}{r}\right)^{1/2} E_{(\theta)}, \\
 E_\varphi &= r \sin \theta \left(1 - \frac{2}{r}\right)^{1/2} E_{(\varphi)}, \\
 J^r &= \left(1 - \frac{2}{r}\right)^{1/2} J^{(r)}, \\
 J^\theta &= \frac{1}{r} J^{(\theta)}, \\
 J^\varphi &= \frac{1}{r \sin \theta} J^{(\varphi)} + \frac{2a}{r^3} \left(1 - \frac{2}{r}\right)^{-1/2} J^{(t)}, \\
 J^t &= \left(1 - \frac{2}{r}\right)^{-1/2} J^{(t)}.
 \end{aligned}
 \tag{4}$$

2.1.2. Innermost stable circular orbit

The minimum allowed radius of charged particle trajectory that is able to maintain stable circular orbit and do not enter into event horizon of black hole is called innermost stable circular orbit (ISCO). In the accretion disc theory, ISCO is regarded as one of the rotating black hole’s important features such as event horizon and ergosphere. ISCO is expected to be the inner edge of an accretion disc that rotates around a black hole. The radius of ISCO is 6 m in the case of a Schwarzschild black hole, while for a Kerr black hole, it is dependent on the black hole’s spin by the following formula:

$$\begin{aligned}
 Z_1 &= 1 + (1 - a^2)^{1/3} [(1 + a)^{1/3} + (1 - a)^{1/3}], \\
 Z_2 &= \sqrt{3a^2 + Z_1^2}, \\
 r_{\text{ISCO}} &= 3 + Z_2 - \sqrt{(3 - Z_1)(3 + Z_1 + 2Z_2)}.
 \end{aligned}$$

In our model, we adopt the spherical coordinates of (r, θ, φ) , defining the polar axis $\theta = 0$ and $\theta = \pi$ to be perpendicular to the disc plane. We set a computational domain of $r_{\text{ISCO}} \leq r \leq 50$ m and $\frac{\pi}{6} \leq \theta \leq \pi - \frac{\pi}{6}$. We draw the schematic depiction of our disc in Figure 1. It shows that the meridional structure of the disc extends to about $\frac{\pi}{3}$ on either side of the equatorial plane. These ranges for the radius r and angular thickness of the disc are assumed typically. Although, as we will see later, some physical circumstances will vary these intervals.

2.1.3. Keplerian velocity distribution

In Newtonian gravity, angular momentum l^* and angular velocity Ω are related by the formula $l^* = r^2 \Omega$, and therefore, there is no ambiguity in defining a non-rotating frame as $\Omega = 0 = l^*$. However, in the rotating Kerr geometry $l^* \propto (\Omega - \omega)$, wherein $\Omega = \frac{d\varphi}{dt}$ is the angular velocity of the orbiting matter and $\omega = -\frac{g_{t\varphi}}{g_{\varphi\varphi}} = \frac{2a}{r^3}$ is that of the frame dragging of the LNRF relative to distant observers. Generally, the azimuthal component of the 3-velocity in the LNRF reads $V^{(\varphi)} = \frac{dx^{(\varphi)}}{dx^{(0)}}$, where $x^{(0)}$ and $x^{(\varphi)}$ are the time and spatial coordinates in the LNRF, respectively,

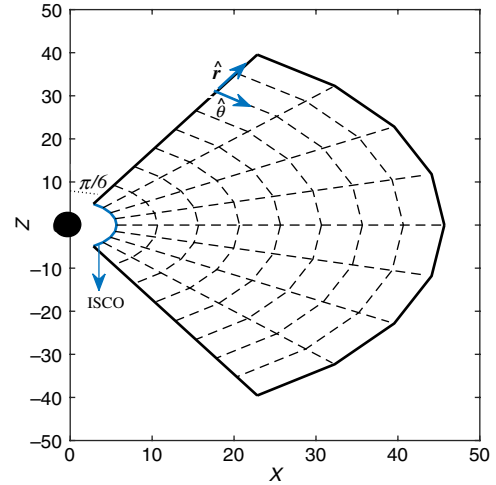


Figure 1. Schematic sketch of the disc with the central black hole.

$$\begin{aligned}
 dx^{(0)} &= \lambda_i^{(0)} dx^i = \left(1 - \frac{2}{r}\right)^{1/2} dt, \\
 dx^{(\varphi)} &= \lambda_i^{(\varphi)} dx^i = r \sin \theta [d\varphi - \omega dt].
 \end{aligned}$$

Afterwards,

$$V^{(\varphi)} = r \sin \theta \left(1 - \frac{2}{r}\right)^{-1/2} [\Omega - \omega].$$

If the matter follows nearly circular orbits characterised by the Keplerian distributions of the angular velocity

$$\Omega_K = \frac{1}{r^{3/2} + a},$$

then the azimuthal component of the Keplerian 3-velocity in the LNRF is obtained as

$$V_K^{(\varphi)} = r \sin \theta \left(1 - \frac{2}{r}\right)^{-1/2} \left(\frac{1}{r^{3/2} + a} - \frac{2a}{r^3}\right).$$

2.2. Seed magnetic field model

As a matter of fact, in problem of magnetised accretion discs, the magnetic field of a resistive disc is not totally arisen from the electric current of the plasma disc. Strength of the disc current is determined in agreement with that of the external field as well. In such a situation, there is always an external field penetrating the disc (Kaburaki 1987). We describe the magnetic field as a superposition of the seed field B^S caused by some external sources and the disc field B^D induced by the current flowing in the disc

$$\mathbf{B} = \mathbf{B}^S + \mathbf{B}^D.$$

Roughly speaking, magnetosphere develops well in the place where the strength of the seed field exceeds that of the disc field (i.e. $|\mathbf{B}^S| \geq |\mathbf{B}^D|$). And also, magnetodisc is the region where $|\mathbf{B}^S| \ll |\mathbf{B}^D|$. Thus, within the disc, \mathbf{B} can be replaced by \mathbf{B}^D , with a good accuracy. In this way, the magnetic field appearing in the next sections is the same as \mathbf{B}^D , that its superscript D has been dropped for simplicity. From now on, we put superscript just for the seed field \mathbf{B}^S .

Realistic cases of a rotating black hole with a disc and magnetic field are likely to be extremely complicated. However, some

authors have discussed the magnetic field associated with the black hole as a somewhat poloidal structure and have modelled it as being generated by some toroidal electric current rings exterior to the black hole’s event horizon (Li 2000; Ghosh 2000; Tomimatsu & Takahashi 2001). We apply this poloidal structure as a dipolar model for the seed magnetic field (Prasanna & Vishveshwara 1978; Takahashi & Koyama 2009)

$$B_{(r)}^S = -\frac{3\mu}{4\gamma^2} \frac{2 \cos \theta}{r^2 \Sigma} \left\{ W \left(1 + \frac{a^2 \sin^2 \theta}{\Sigma} \right) - \sin^2 \theta \left[(r-1)a^2 - \frac{\Delta a^2}{2\gamma} \ln \left(\frac{r-r_-}{r-r_+} \right) \right] \right\},$$

$$B_{(\theta)}^S = \frac{3\mu}{4\gamma^2} \left(1 - \frac{2}{r} \right)^{1/2} \frac{1}{r\Sigma} \left(\frac{-2rW}{\Sigma} + \frac{\partial W}{\partial r} \right) \sin \theta.$$

Here, μ is the magnetic dipole moment of the central black hole which relates to its surface magnetic field B_s and radius R as $\mu = B_s R^3$. We take $\mu = 1260 \times 10^{27}$ Gauss.cm³, that is, an appropriate choice for the intrinsic magnetic moment of a typical 10 M_⊙ black hole (Robertson & Leiter 2002). It is worth noting that Σ and Δ have the previous definitions and the other undefined variables are

$$r_{\pm} = 1 \pm \gamma,$$

$$\gamma = \sqrt{1 - a^2},$$

$$Q = \frac{1}{2\gamma} \ln \left(\frac{r-r_-}{r-r_+} \right),$$

$$W = (r-1)a^2 \cos^2 \theta + r(r^2 + r + 2a^2) - [r(r^3 - 2a^2 + a^2r) + \Delta a^2 \cos^2 \theta] Q,$$

$$\frac{\partial W}{\partial r} = a^2 \cos^2 \theta + 3r^2 + 2r + 2a^2 - [4r^3 - 2a^2 + 2a^2r + 2a^2 \cos^2 \theta (r-1)] Q + [r(r^3 - 2a^2 + a^2r) + \Delta a^2 \cos^2 \theta] \frac{1}{(r-1)^2 - \gamma^2}.$$

Figure 2 shows a typical profile of the dipolar magnetic field structure of central black hole at infinity (Appendix A).

3. General formalism

3.1. Basic equation

Fully general relativistic MHD equations governing the motion of the resistive magnetised plasma accreted by a central compact object are mass conservation or continuity equation

$$(\rho_0 u^i)_{;i} = 0, \tag{5}$$

and energy–momentum conservation law

$$T^i_{;j} = 0, \tag{6}$$

supplemented by Maxwell equations

$$F^i_{;j} = -4\pi J^i, \tag{7}$$

$$F_{ij,k} + F_{ki,j} + F_{jk,i} = 0, \tag{8}$$

and the generalised Ohm’s law

$$J^i = \sigma F^i_k u^k, \tag{9}$$

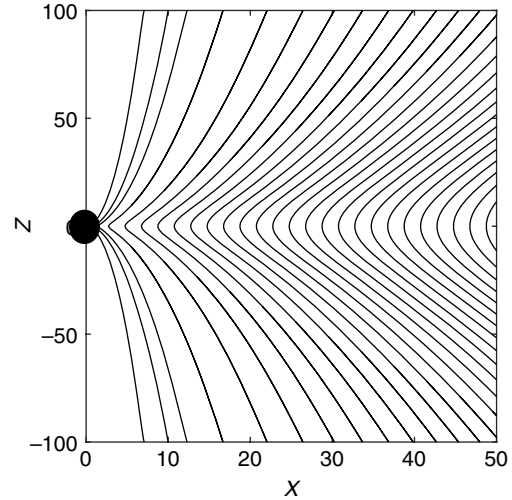


Figure 2. Dipolar magnetic field model of the central black hole in the meridional plane.

wherein σ is the electric conductivity which is assumed constant for simplicity. It is worth noting here that semicolon stands for covariant derivative and comma for partial derivative. Latin indices denote spacetime components (0–3) and Greek ones denote spatial components (1–3). Furthermore, we adopt the standard convention for the summation over the repeated indices.

Our MHD system will be specified by the following choice for the energy–momentum tensor

$$T^{ij} = T^{ij}_{\text{Fluid}} + T^{ij}_{\text{Em}}.$$

It consists of a fluid part

$$T^{ij}_{\text{Fluid}} = (\rho + p) u^i u^j - p g^{ij},$$

and an electromagnetic part

$$T^{ij}_{\text{Em}} = -\frac{1}{4\pi} \left(F^{ik} F^j_k - \frac{1}{4} g^{ij} F_{kl} F^{kl} \right),$$

where p is the gas pressure and $\rho = \rho_0 + u$ is the total density of mass–energy including the rest mass density ρ_0 and the internal energy per unit volume u . On the other hand, the electromagnetic field tensor is related to the electric and magnetic fields through

$$E_\alpha = F_{\alpha t}, \quad B_\alpha = \epsilon_{\alpha\beta\gamma} F_{\beta\gamma},$$

where $\epsilon_{\alpha\beta\gamma}$ is the Levi-Civita symbol. For an axisymmetric and stationary magnetofluid disc, all flow variables that neither depend on the time t nor on the azimuthal coordinate φ are functions of only r and θ . Then, equations (7) and (8) may be expanded

$$4\pi J^r = -\frac{1}{r^2 \sin \theta} \left(1 - \frac{2}{r} \right) \frac{\partial}{\partial \theta} (\sin \theta B_\varphi), \tag{10}$$

$$4\pi J^\theta = \frac{1}{r^2} \frac{\partial}{\partial r} \left[\left(1 - \frac{2}{r} \right) B_\varphi \right], \tag{11}$$

$$4\pi J^\varphi = \frac{1}{r^4 \sin \theta} \frac{\partial}{\partial \theta} \left(\frac{B_r}{\sin \theta} \right) - \frac{1}{r^2 \sin^2 \theta} \frac{\partial}{\partial r} \left[\left(1 - \frac{2}{r} \right) B_\theta \right]$$

$$- \frac{2a}{r^2} \left[\frac{\partial}{\partial r} \left(\frac{E_r}{r} \right) + \frac{1}{r^3 \sin \theta} \left(1 - \frac{2}{r} \right)^{-1} \frac{\partial}{\partial \theta} (\sin \theta E_\theta) \right], \tag{12}$$

$$4\pi J^t = -\frac{1}{r^2} \frac{\partial}{\partial r} (r^2 E_r) - \frac{1}{r^2 \sin \theta} \left(1 - \frac{2}{r}\right)^{-1} \frac{\partial}{\partial \theta} (\sin \theta E_\theta) - \frac{2a}{r^5 \sin \theta} \left(1 - \frac{2}{r}\right)^{-1} \frac{\partial}{\partial \theta} (\sin \theta B_r) + \frac{2a}{r^2} \frac{\partial}{\partial r} \left(\frac{B_\theta}{r}\right), \quad (13)$$

$$\frac{\partial B_\theta}{\partial \theta} + \frac{\partial B_r}{\partial r} = 0, \quad (14)$$

$$\frac{\partial E_\theta}{\partial r} - \frac{\partial E_r}{\partial \theta} = 0, \quad (15)$$

$$\frac{\partial E_\varphi}{\partial r} = 0, \quad (16)$$

$$\frac{\partial E_\varphi}{\partial \theta} = 0. \quad (17)$$

3.2. Possible solutions

3.2.1. Simplifying assumptions

Equations (16) and (17) state that the toroidal electric field must be constant. This constant value may be chosen equal to zero for simplicity. Now, we need a wise assumption to simplify the highly non-linear coupled equations (9)–(15). If we assume

$$B_\varphi = \frac{b_\varphi}{\sin \theta} \left(1 - \frac{2}{r}\right)^{-1}, \quad (18)$$

wherein b_φ is constant, then $J^r = J^\theta = 0$ through equations (10) and (11). Also through the Ohm's law (9), it results in

$$E_r = B_\theta V^\varphi - B_\varphi V^\theta, \\ E_\theta = -B_r V^\varphi + B_\varphi V^r,$$

that keep the same forms in LNRF as

$$E_{(r)} = B_{(\theta)} V^{(\varphi)} - B_{(\varphi)} V^{(\theta)}, \quad (19)$$

$$E_{(\theta)} = -B_{(r)} V^{(\varphi)} + B_{(\varphi)} V^{(r)}. \quad (20)$$

The other non-zero components of the Ohm's law (9) gives

$$J^\varphi = -\sigma (B_\theta u^r - B_r u^\theta) \left[\frac{1}{r^2 \sin^2 \theta} + \frac{2a}{r^3} \left(1 - \frac{2}{r}\right)^{-1} V^\varphi \right],$$

$$J^t = -\sigma \left(1 - \frac{2}{r}\right)^{-1} (B_\theta u^r - B_r u^\theta) \left(V^\varphi - \frac{2a}{r^3} \right) \\ = -\frac{\sigma}{r \sin \theta} \left(1 - \frac{2}{r}\right)^{-1/2} (B_\theta u^r - B_r u^\theta) V^{(\varphi)},$$

that they find a more concise form, with the help of transformations (4)

$$J^{(\varphi)} = -\sigma u^0 \left(1 - \frac{2}{r}\right)^{1/2} [B_{(\theta)} V^{(r)} - B_{(r)} V^{(\theta)}], \quad (21)$$

$$J^{(t)} = J^{(\varphi)} V^{(\varphi)}. \quad (22)$$

Defining the total derivative

$$D \equiv V^{(r)} \frac{\partial}{\partial r} + \left(1 - \frac{2}{r}\right)^{-1/2} \frac{V^{(\theta)}}{r} \frac{\partial}{\partial \theta},$$

and combining equation (5) and the zeroth component of equation (6), continuity equation is achieved in LNRF

$$(\rho + p) \left\{ \frac{\partial V^{(r)}}{\partial r} + \frac{2}{r} V^{(r)} + \frac{1}{r} \left(1 - \frac{2}{r}\right)^{-1/2} \left[\frac{\partial V^{(\theta)}}{\partial \theta} + \cot \theta V^{(\theta)} \right] + \frac{6a}{r^3} \left(1 - \frac{2}{r}\right)^{-1/2} \sin \theta V^{(r)} V^{(\varphi)} \right\} + D(\rho - p) = \frac{2}{\sigma u^0} \left(1 - \frac{2}{r}\right)^{-1} [J^{(\varphi)}]^2 \{1 - [V^{(\varphi)}]^2\}, \quad (23)$$

and also the momentum equations are obtained from the spatial components of equation (6)

$$(\rho + p) (1 - V^2)^{-1} \left[DV^{(r)} - \frac{1}{r} \{ [V^{(\theta)}]^2 + [V^{(\varphi)}]^2 \} + \frac{1}{r^2} \left(1 - \frac{2}{r}\right)^{-1} \{1 - [V^{(r)}]^2\} - \frac{6a}{r^3} \left(1 - \frac{2}{r}\right)^{-1/2} \sin \theta V^{(\varphi)} \{1 - [V^{(r)}]^2\} \right] + \frac{\partial p}{\partial r} - \left(1 - \frac{2}{r}\right)^{-1/2} J^{(\varphi)} B_{(\theta)} \{1 - [V^{(\varphi)}]^2\} = 0, \quad (24)$$

$$(\rho + p) (1 - V^2)^{-1} \left\{ DV^{(\theta)} + \frac{(1 - \frac{3}{r}) V^{(r)} V^{(\theta)}}{(1 - \frac{2}{r}) r} + \frac{6a}{r^3} \left(1 - \frac{2}{r}\right)^{-1/2} \sin \theta V^{(r)} V^{(\theta)} V^{(\varphi)} - \cot \theta \left(1 - \frac{2}{r}\right)^{-1/2} \frac{[V^{(\varphi)}]^2}{r} \right\} + \left(1 - \frac{2}{r}\right)^{-1/2} \frac{1}{r} \frac{\partial p}{\partial \theta} + \left(1 - \frac{2}{r}\right)^{-1/2} B_{(r)} J^{(\varphi)} \{1 - [V^{(\varphi)}]^2\} = 0, \quad (25)$$

$$DV^{(\varphi)} + \left(1 - \frac{2}{r}\right)^{-1} \left(1 - \frac{3}{r}\right) \frac{V^{(r)} V^{(\theta)}}{r} + \cot \theta \left(1 - \frac{2}{r}\right)^{-1/2} \frac{V^{(\theta)} V^{(\varphi)}}{r} + \frac{6a}{r^3} \left(1 - \frac{2}{r}\right)^{-1/2} \sin \theta V^{(r)} [V^{(\varphi)}]^2 = 0. \quad (26)$$

Equation (26) may be summarised as

$$D\tilde{V}^{(\varphi)} = -\frac{6a}{r^4} V^{(r)} [\tilde{V}^{(\varphi)}]^2, \quad (27)$$

while we define a new variable

$$\tilde{V}^{(\varphi)} = r \sin \theta \left(1 - \frac{2}{r}\right)^{-1/2} V^{(\varphi)}.$$

To have an integrable form for equation (27), we multiply both its sides, by an integration constant L ,

$$L \frac{D\tilde{V}^{(\varphi)}}{[\tilde{V}^{(\varphi)}]^2} = -D \left(1 - \frac{2aL}{r^3}\right).$$

Now, it can integrate simply as

$$\tilde{V}^{(\varphi)} = L \left(1 - \frac{2aL}{r^3}\right)^{-1}.$$

Indeed, due to the dimensional considerations, L is defined as $L = lm c$, wherein l is called the angular momentum parameter. Ultimately, the final solution for the azimuthal velocity is obtained

$$V^{(\varphi)} = \frac{L}{r \sin \theta} \left(1 - \frac{2}{r}\right)^{1/2} \left(1 - \frac{2aL}{r^3}\right)^{-1}. \quad (28)$$

Substituting equations (22) and (28), the transformation equation (4) for J^φ gets a shorter form as

$$J^\varphi = \frac{1}{r \sin \theta} \left(1 - \frac{2aL}{r^3}\right)^{-1} J^{(\varphi)}.$$

To brief the appearance of the governing equations (23)–(26), we multiply equation (24) by $V^{(r)}$, equation (25) by $V^{(\theta)}$, and equation (26) by $V^{(\varphi)}$ and adding

$$\begin{aligned} &(\rho + p) D \ln \left[\left(1 - \frac{2}{r}\right) \left(1 - \frac{2aL}{r^3}\right)^{-2} (1 - V^2)^{-1} \right] \\ &+ 2 D p = -\frac{2}{\sigma u^0} \left(1 - \frac{2}{r}\right)^{-1} [J^{(\varphi)}]^2 \{1 - [V^{(\varphi)}]^2\}. \end{aligned} \quad (29)$$

Continuity equation (23) can be simplified too

$$\begin{aligned} &(\rho + p) \left[\nabla \cdot \tilde{V} + D \ln \left(1 - \frac{2aL}{r^3}\right) \right] + D(\rho - p) \\ &= \frac{2}{\sigma u^0} \left(1 - \frac{2}{r}\right)^{-1} [J^{(\varphi)}]^2 \{1 - [V^{(\varphi)}]^2\}, \end{aligned} \quad (30)$$

with a new definition for total fluid velocity as

$$\tilde{V} = V^{(r)} \hat{r} + \tilde{V}^{(\theta)} \hat{\theta} + V^{(\varphi)} \hat{\phi}, \quad (31)$$

wherein $\tilde{V}^{(\theta)} = V^{(\theta)} \left(1 - \frac{2}{r}\right)^{-1/2}$. As seen, right-hand side of these latter two equations (29) and (30) are similar with opposite sign. It motivates us to add them to get rid of this long term

$$\nabla \cdot \tilde{V} + D \ln \left[\frac{(\rho + p) \left(1 - \frac{2}{r}\right)}{\left(1 - \frac{2aL}{r^3}\right) (1 - V^2)} \right] = 0. \quad (32)$$

Therefore, we have summarised the motion equations (23)–(26) in an equation (32). To achieve an integrable form for it, we must try to write the term $\nabla \cdot \tilde{V}$ in terms of the total derivative D . This term may be written as

$$\nabla \cdot \tilde{V} = D \ln (r^2 \sin \theta V^{(r)}) + \frac{\tilde{V}^{(\theta)}}{r} \frac{\partial}{\partial \theta} \ln \left(\frac{\tilde{V}^{(\theta)}}{V^{(r)}} \right).$$

In order to reach to an integrable form, we try to express the second term in terms of D . To this aim, one may assume that the poloidal component of total fluid velocity including $V^{(r)}$ and $\tilde{V}^{(\theta)}$ are two separable functions of their independent variables r and θ as $V^{(r)} = V_1^{(r)}(r) V_2^{(r)}(\theta)$ and $\tilde{V}^{(\theta)} = V_1^{(\theta)}(r) V_2^{(\theta)}(\theta)$, respectively. Now, if their radial dependencies are presumed to be similar [i.e. $V_1^{(r)}(r) = V_1^{(\theta)}(r)$], then the term $\frac{\tilde{V}^{(\theta)}}{V^{(r)}}$ is a function only of θ as

$$\frac{\tilde{V}^{(\theta)}}{V^{(r)}} = \frac{1}{C_1(\theta)}, \quad (33)$$

and equation (32) is rewritten as

$$D \ln \left[\frac{(\rho + p) \left(1 - \frac{2}{r}\right)}{\left(1 - \frac{2aL}{r^3}\right) (1 - V^2)} r^2 \sin \theta V^{(r)} \right] - D \ln C_1(\theta) = 0. \quad (34)$$

In fact, the term in bracket can be interpreted as mass accretion rate (Shaghaghian 2016)

$$\dot{M} = \frac{(\rho + p) \left(1 - \frac{2}{r}\right)}{\left(1 - \frac{2aL}{r^3}\right) (1 - V^2)} r^2 \sin \theta V^{(r)}. \quad (35)$$

Thus, equation (34) leads to

$$\dot{M} = \dot{M}_0 C_1(\theta), \quad (36)$$

wherein \dot{M}_0 is an integration constant and $C_1(\theta)$ is an unknown function that will be determined. We prefer a sub-Eddington regime. Since as elucidates in the introduction, the super-Eddington accretion discs are generally expected to possess vortex funnels and radiation pressure driven jets (Okuda 2002). Although this aspect is so noteworthy in recent decades, it is beyond the scope of this paper and must be pursued separately. Thus, we choose $\dot{M}_0 = -10^{-8} \frac{M_\odot}{\text{year}}$, which is a normal mass accretion rate for a typical $M = 10 M_\odot$ black hole (Koide 2010).

3.2.2. Disc magnetic field model

Now, it is time to return to the remaining Maxwell equations (12)–(15) and rewrite them in LNRF with the aid of transformation equations (4),

$$\begin{aligned} 4\pi J^{(\varphi)} &= \frac{1}{r} \left(1 - \frac{2aL}{r^3}\right) \left[\frac{\partial B_{(r)}}{\partial \theta} - \frac{\partial}{\partial r} \left[r \left(1 - \frac{2}{r}\right)^{1/2} B_{(\theta)} \right] \right. \\ &\quad \left. - \frac{2a}{r} \left\{ r \sin \theta \frac{\partial}{\partial r} \left[\frac{E_{(r)}}{r} \right] \right. \right. \\ &\quad \left. \left. + \frac{1}{r} \left(1 - \frac{2}{r}\right)^{-1/2} \frac{\partial}{\partial \theta} [\sin \theta E_{(\theta)}] \right\} \right], \end{aligned} \quad (37)$$

$$4\pi J^{(t)} = \frac{-1}{r^2} \left(1 - \frac{2}{r}\right)^{1/2} \frac{\partial}{\partial \theta} [r^2 E_{(r)}] - \frac{1}{r \sin \theta} \frac{\partial}{\partial \theta} [\sin \theta E_{(\theta)}]. \quad (38)$$

$$\sin \theta \frac{\partial}{\partial r} [r^2 B_{(r)}] + r \left(1 - \frac{2}{r}\right)^{-1/2} \frac{\partial}{\partial \theta} [\sin \theta B_{(\theta)}] = 0, \quad (39)$$

$$\frac{\partial}{\partial r} [A B_{(r)}] + \frac{1}{r} \left(1 - \frac{2}{r}\right)^{-1/2} \frac{\partial}{\partial \theta} [A B_{(\theta)}] = 0, \quad (40)$$

where

$$A = \frac{2a}{r} \sin \theta + r \left(1 - \frac{2}{r}\right)^{1/2} V^{(\varphi)}.$$

As expected, due to the relations (19), (20), and (22), equations (37) and (38) are not independent and achieve a similar

appearance

$$\begin{aligned}
 4\pi J^{(\varphi)} = & \frac{1}{r} \frac{\partial B(r)}{\partial \theta} - \frac{1}{r} \frac{\partial}{\partial r} \left[r \left(1 - \frac{2}{r} \right)^{1/2} B_{(\theta)} \right] \\
 & + \frac{6aL}{r^4} \left(1 - \frac{2}{r} \right)^{1/2} \left(1 - \frac{2aL}{r^3} \right)^{-1} B_{(\theta)} \\
 & + \frac{2a}{r^2} \left(1 - \frac{2aL}{r^3} \right) \left\{ r \sin \theta \frac{\partial}{\partial r} \left[B_{(\varphi)} \frac{V^{(\theta)}}{r} \right] \right. \\
 & \left. - \frac{1}{r} \left(1 - \frac{2}{r} \right)^{-1/2} \frac{\partial}{\partial \theta} [\sin \theta B_{(\varphi)} V^{(r)}] \right\}. \quad (41)
 \end{aligned}$$

b_φ as a free parameter is chosen small, so that the last term in $J^{(\varphi)}$ [equation (41)] may be ignorable. Because it is the product of two small parameters a and b_φ .

Poloidal magnetic field of the disc is usually achieved through the self-consistent solution of equations (39) and (40). This is what happens in the case of Schwarzschild metric (Shaghaghian 2016). However, in the case of Kerr metric, by virtue of the presence of the term $\frac{2a}{r} \sin \theta$ in A , the self-consistent solution that satisfies these two equations simultaneously is not possible. Consequently, to find the poloidal magnetic field, they have to be solved separately (Shaghaghian 2011). As a result, we go to equation (39) which seems to be easier to solve. To this aim, we presume the following model for the poloidal component of the disc's magnetic field

$$\begin{aligned}
 B(r) &= b_1(r) \cot \theta b_2(\theta), \\
 B_{(\theta)} &= f(r) b_1(r) b_2(\theta),
 \end{aligned}$$

here

$$b_1(r) = -B_1 r^{k-2} \left(1 - \frac{2}{r} \right)^{-k/2} \left(1 - \frac{2aL}{r^3} \right)^k,$$

wherein k and B_1 are constants and $b_2(\theta)$ and $f(r)$ are the unknown functions that must be determined. It is valuable to mention that this model is inspired us by the self-consistent solution for poloidal magnetic field in the Schwarzschild metric (Shaghaghian 2016). Substituting this model in equation (39), we have

$$\frac{\left(1 - \frac{2}{r} \right)^{1/2}}{r f(r) b_1(r)} \frac{d}{dr} [r^2 b_1(r)] + \frac{1}{b_2(\theta) \cos \theta} \frac{d}{d\theta} [\sin \theta b_2(\theta)] = 0.$$

As seen, functions of the variables r and θ have been separated. Thus, each part must be constant

$$\begin{aligned}
 \frac{d [\sin \theta b_2(\theta)]}{b_2(\theta)} &= k \cos \theta d\theta, \\
 f(r) &= \frac{1}{-kr b_1(r)} \left(1 - \frac{2}{r} \right)^{1/2} \frac{d}{dr} [r^2 b_1(r)].
 \end{aligned}$$

Solving these two equations, the unknown functions in our model are obtained

$$\begin{aligned}
 b_2(\theta) &= \sin^{k-1} \theta, \\
 f(r) &= - \left(1 - \frac{2}{r} \right)^{-1/2} A_1(r).
 \end{aligned}$$

wherein

$$A_1(r) = \left[\left(1 - \frac{3}{r} \right) + \frac{6aL}{r^3} \left(1 - \frac{2}{r} \right) \left(1 - \frac{2aL}{r^3} \right)^{-1} \right].$$

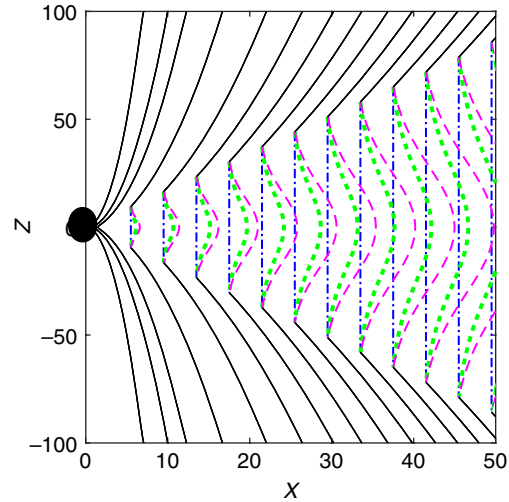


Figure 3. Structure of magnetic field lines in presence of disc field projected on the meridional plane of the disc. The solid lines being the same as Figure 2 represent the dipolar magnetic field of the central black hole, while the dashed lines represent the disc's field in the case $b_\varphi = 0$. The different colours correspond to the different spin parameter a : blue - - is $a = 0$, green dotted is $a = 0.1$, and magenta - - - denotes $a = 0.2$.

Then, the components of the poloidal magnetic field are achieved

$$B(r) = -B_1 r^{k-2} \frac{\left(1 - \frac{2aL}{r^3} \right)^k}{\left(1 - \frac{2}{r} \right)^{k/2}} \sin^{k-2} \theta \cos \theta, \quad (42)$$

$$B_{(\theta)} = B_1 r^{k-2} \frac{\left(1 - \frac{2aL}{r^3} \right)^k}{\left(1 - \frac{2}{r} \right)^{(k+1)/2}} A_1(r) \sin^{k-1} \theta. \quad (43)$$

B_1 is a definite constant that may be found as a result of continuity of the magnetic field lines across the disc boundary surface

$$(B^D)^2 |_{r=r_0, \theta=\frac{\pi}{6}} = (B^S)^2 |_{r=r_0, \theta=\frac{\pi}{6}}, \quad (44)$$

where

$$\begin{aligned}
 (B^D)^2 &= B_r^2 + B_\theta^2, \\
 (B^S)^2 &= [B_r^S]^2 + [B_\theta^S]^2,
 \end{aligned}$$

and r_0 is the radius where two field lines connect together. Ghosh & Lamb (1979a, b) notified that the external magnetic field penetrates the disc via a variety of processes owing to the presence of a finite resistivity. In fact, electrical conductivity is treated as a measure of the rate of field line slippage through the plasma disc. Figure 3 shows the magnetic field lines of the disc connected with the undistorted dipolar magnetic field lines of the central hole at the surface of the disc. Additionally, it is evident that the magnetic field lines inside the disc are pushed outwards. As black hole spins faster, this outward push becomes more (Appendix A).

Now, we profit this occasion and define the magnetic pressure both in the disc as $p_{\text{mag}}^D = \frac{(B^D)^2}{8\pi}$ and within the magnetosphere surrounding the central black hole as $p_{\text{mag}}^S = \frac{(B^S)^2}{8\pi}$. We study the effect of disc magnetic pressure via a new physical variable β defined as the ratio of the gas pressure to the magnetic pressure in the disc. Thus, $\beta = \frac{p}{p_{\text{mag}}^D}$.

3.2.3. Analytical and numerical solutions

Substituting equations (42) and (43) in equation (41), the azimuthal current density is obtained

$$J^{(\varphi)} = -\frac{B_1}{4\pi} Y(r, \theta) r^{k-3} \frac{\left(1 - \frac{2aL}{r^3}\right)^k}{\left(1 - \frac{2}{r}\right)^{k/2}} \sin^{k-1} \theta, \quad (45)$$

in which

$$Y(r, \theta) = \left\{ (k-2) \cot^2 \theta - 2 \left(1 - \frac{3}{r}\right) + k \frac{\left(1 - \frac{3}{r}\right)^2}{\left(1 - \frac{2}{r}\right)} + \frac{6aL}{\left(1 - \frac{2aL}{r^3}\right)} \left[-5 + \frac{7}{r} + 2k \left(1 - \frac{3}{r}\right) \right] \right\}.$$

We have derived two different expressions for the current density $J^{(\varphi)}$ [equations (21) and (45)]. Evidently, they have to be consistent

$$V^{(r)} A_1(r) + \left(1 - \frac{2}{r}\right) \cot \theta \tilde{V}^{(\theta)} = \frac{1}{4\pi\sigma u^0} \frac{Y(r, \theta)}{r}. \quad (46)$$

Employing the assumption $V^{(r)} = C_1(\theta) \tilde{V}^{(\theta)}$ [equation (33)] and the definition of u^0 [equation (3)], in the above equation, it gives the meridional velocity as

$$\tilde{V}^{(\theta)} = S_0 \sqrt{I} Y, \quad (47)$$

wherein $S_0 = \frac{-1}{4\pi\sigma}$ has the dimension of magnetic diffusivity and

$$I = \frac{1 - [V^{(\varphi)}]^2}{S_1^2 + (S_0 Y)^2 \left[\left(1 - \frac{2}{r}\right) + C_1^2(\theta) \right]},$$

$$S_1 = A_1(r) r \left(1 - \frac{2}{r}\right)^{-1/2} C_1(\theta) + r \left(1 - \frac{2}{r}\right)^{1/2} \cot \theta.$$

Function Y has a zero in a point between $k = 2$ and $k = 3$ for all grid points in Figure 1. For $k > 2$, it is positive ($Y > 0$) and for $k \leq 2$, it is negative ($Y < 0$). If we choose the second set ($k \leq 2$ and $Y < 0$), then as above, S_0 must be negative, so that the vertical velocity is positive to indicate inflows. If the first set ($k > 2$ and $Y > 0$) is chosen, the only difference will be in the sign of S_0 that must be positive. Continuation of the story is the same as other set.

Up to now, both the radial and meridional velocities and the mass accretion rate have been obtained in terms of $C_1(\theta)$. To define this unknown function, we aid from the integrability condition of pressure

$$\frac{\partial^2 p}{\partial r \partial \theta} = \frac{\partial^2 p}{\partial \theta \partial r}.$$

It provides a second-order ordinary differential equation for $C_1(\theta)$ as

$$\frac{d^2 C_1(\theta)}{d\theta^2} = \Psi(r, \theta),$$

where $\Psi(r, \theta)$ is a known function of r and θ in terms of $C_1(\theta)$ and $\frac{dC_1(\theta)}{d\theta}$ that have been derived in Appendix B. The above differential equation can be solved numerically with appropriate boundary conditions. Integration is initiated from the upper boundary surface (i.e. $\theta = \pi/6$) with the following boundary condition

$$C_1(\theta) \Big|_{\theta=\frac{\pi}{6}} = 0.1, \quad \& \quad \frac{dC_1(\theta)}{d\theta} \Big|_{\theta=\frac{\pi}{6}} = 1.$$

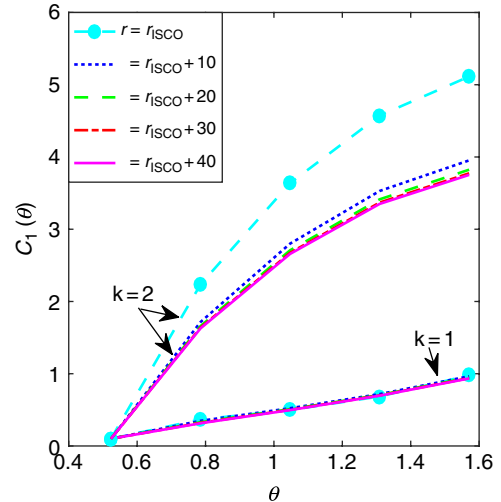


Figure 4. Profiles of $C_1(\theta)$ at the different dimensionless radial distances shown in the key for two values of k . The other constant parameters are $a = 0.1$, $l = 1$, $\sigma = 10$, and $\dot{M}_0 = -10^{-8} \frac{M_\odot}{\text{year}}$.

After running a complicated code, C_1 is achieved as an ascending function of θ (Figure 4). C_1 has been presumed to be dependent just on θ . Thus, we have to choose the set of free parameters as well as the boundary conditions in the manner that C_1 's profiles in different radii are coincident. Otherwise, the relevant radii must omit from our allowed radial interval. This point determines for us the allowed radius for the inner edge of our disc. For instance, we discuss two sets of free parameters employed in plotting Figure 4. For the set $k = 1$, we choose r_{ISCO} as the inner edge (i.e. $r_{\text{in}} = r_{\text{ISCO}}$). However, for the set $k = 2$, we choose $r_{\text{in}} = r_{\text{ISCO}} + 10$. On account of this fact that for $k = 2$, C_1 's profile in r_{ISCO} is not coincident on the others, but 10 units farther than ISCO, our expectation about independency of C_1 on the radial distance r is almost satisfied.

With specified $C_1(\theta)$, we can obtain the radial and meridional velocities, and mass accretion rate through equations (33), (47), and (36), respectively. Both radial velocity and mass accretion rate must be negative. This negativity indicates the inflow towards the central black hole. Because, the positive radial direction is defined in the direction of increasing r . Moreover, the positive meridional direction is defined in the direction of increasing θ too (Figure 1). Therefore, the negative meridional velocity denotes outflow which is beyond the scope of this paper. Whereas the radial inflow velocity must be negative and the meridional velocity must be positive, then we rewrite equation (33) as

$$V^{(r)} = -C_1(\theta) \tilde{V}^{(\theta)}.$$

At this time, there remains just two unknown physical variables, gas pressure and total density. Gas pressure may be achieved from the pressure gradient terms in momentum equations [(24) or (25)]. After some manipulations, these two equations change to equations (B1) and (B2). We prefer to employ the radial component of pressure gradient [equation (B1)], due to its simplicity in integration. Because, $C_1(\theta)$ behaves like a constant in radial integration. It can be rewritten as

$$\frac{\partial p}{\partial r} = \chi(r, \theta). \quad (48)$$

In fact, we rename the right side of equation (B1) as $\chi(r, \theta)$, which is a known function of r and θ . Now, the gas pressure as a function

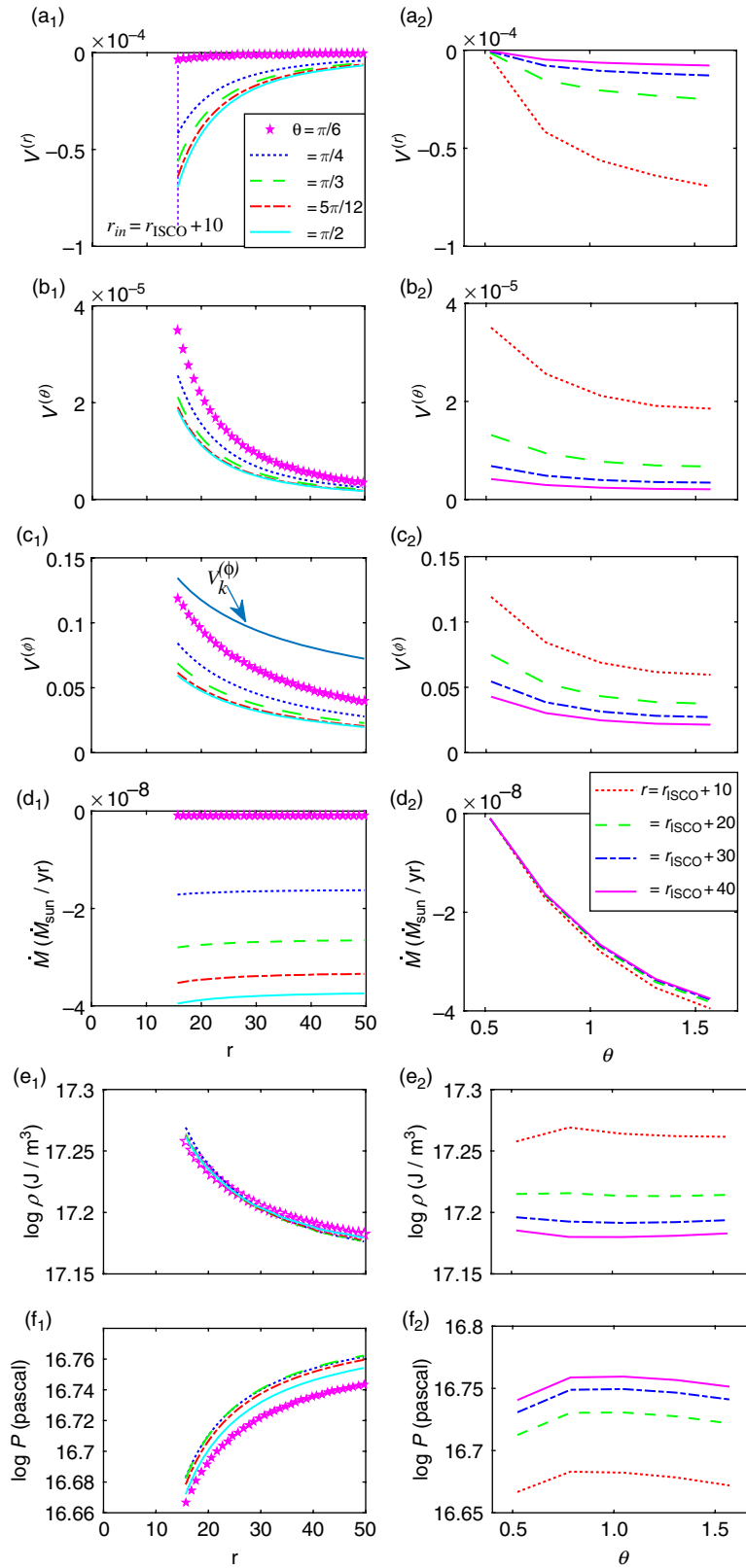


Figure 5. Variation of (a) radial, (b) meridional, and (c) azimuthal velocities, in addition to (d) mass accretion rate, (e) total density, and (f) gas pressure along the radial direction r at the different meridional layers shown in the key (left column) and also along the meridional direction θ at the different radii shown in the key (right column). The constant parameters are $\alpha = 0.1$, $l = 1$, $\sigma = 10$, $k = 2$, and $\dot{M}_0 = -10^{-8} \frac{M_{\odot}}{\text{year}}$.

of r and θ is obtained by integrating equation (48) with respect to the radial distance,

$$p(r, \theta) = p_{0_{\text{mag}}}^S + \int_{r_{0_{\text{mag}}}}^r \chi(r, \theta) dr. \quad (49)$$

Within the magnetosphere surrounding the black hole, the magnetic pressure dominates. We benefit from this fact to define the integration constant $p_{0_{\text{mag}}}^S$ as the magnetic pressure of the radius $r_{0_{\text{mag}}}$ in the magnetosphere. Besides, total density can be attained through the definition of mass accretion rate [equation (35)]

$$\rho(r, \theta) = \frac{\dot{M}}{r^2 \sin \theta V(r)} \left(\frac{1 - \frac{2aL}{r^3}}{1 - \frac{2}{r}} \right) (1 - V^2) - p. \quad (50)$$

At present, all physical functions of the disc have been specified in terms of some free parameters (i.e. σ , l , a , \dot{M}_0 , and k). An appropriate set of these free parameters is a set that both C_1 does not vary significantly with the radial distance r and the total density is positive throughout the disc. During running the code, it is possible to encounter the situations that for a specific set of free parameters, C_1 is not necessarily independent on r (Figure 4) also the density is negative from a certain radius to the next. Obviously, these features are undesirable to have physically meaningful disc solutions. Hence, in order to avoid these unpleasant cases, we forced to limit the allowed interval for the disc's radius.

Figure 5 gives both radial (left column) and meridional (right column) variations of all the physical quantities of the disc. Close to the inner edge of the disc, all three components of fluid velocity are extremely high and gradually fall off radially outwards (Figure 5a₁, b₁, and c₁). Azimuthal velocity of the surface layer ($\theta = \frac{\pi}{6}$) near ISCO is nearly super-Keplerian and reaches to sub-Keplerian regime in the inner edge ($r_{in} = r_{\text{ISCO}} + 10$). Thus, in our allowed radial interval for $k=2$ solution set, rotation of the disc is sub-Keplerian all over the disc (Figure 5c₁). The horizontal constant lines in Figure 5d₁ are a firm confirmation on the radial independency of mass accretion rate. As we get radially closer to the central black hole, the disc becomes denser (Figure 5e₁); however, its gas pressure falls off rapidly (Figure 5f₁).

From the disc surface ($\theta = \frac{\pi}{6}$) towards the equator ($\theta = \frac{\pi}{2}$), radial inflow including radial velocity (Figure 5a₂) and mass accretion rate (Figure 5d₂) becomes faster. Nonetheless, the meridional (Figure 5b₂) and azimuthal (Figure 5c₂) velocities slow down. The surface layer has a super-Keplerian rotation near ISCO and sub-Keplerian one in the outer edge. The other layers obey the sub-Keplerian regime all over the allowed radius. While the total density remains nearly constant along the meridional direction (Figure 5e₂), pressure ascends from the surface up to around $\theta = \frac{\pi}{4}$, then it becomes constant (Figure 5f₂).

For the solution set $k=1$, as mentioned above, disc starts on ISCO up to around $r=25$. It means that the radius of the disc shrinks in this case with respect to the other set (Figure 6a₁ and b₁). Mass accretion rate and fluid velocity behave in the same manner of the solution set of $k=2$ in the radial and meridional directions. Comparing Figure 6a₁ with Figure 5e₁, it is seen that the ascending behaviour of the total density in the radial direction for the $k=1$ solution set seems to be different with another solution set. Meridional behaviour of the total density in inner region is constant like the $k=2$ solution set. However, in outer region ($r = r_{\text{ISCO}} + 20$), the total density finds the meridional angular dependency (Figure 6a₂). In both solution sets, pressure is an

ascending function of the radial distance. For the set $k=1$, as r increases, pressure tends to remain constant in outer region after an initial ascent (Figure 6b₁). However, for the other set ($k=2$), pressure ascends rapidly towards the outer edge (Figure 5f₁). The meridional behaviour of pressure is just a little different for both sets. It rises uniformly from the surface towards the equator (Figure 6b₂).

Density and pressure coloured distributions have been plotted in Figure 7, as a strong verification on interpretations of profiles of density and pressure in Figure 5e₁, e₂, f₁, and f₂.

In Figure 8, fluid flow has been represented in meridional plane by arrows. The length and direction of the vectors indicate the magnitude and orientation of the total fluid velocity, respectively. Density coloured distribution is seen in the background of this figure as well. The dark blue colour in the right column panels indicates the region with negative density that is a forbidden region. It demonstrates that for the $k=1$ solution set (Figure 8b and d), the radius of the disc shrinks with respect to the other set (Figure 8a and c) and the outer edge becomes nearer to the inner edge resting on ISCO. When rotation of the disc (Figure 5c₁) is a few orders of magnitude faster than the inflow velocity (Figure 5a₁ and b₁), plasma flows in the azimuthal direction (Figure 8a and b). It likes an equilibrium toroidal configuration around the central black hole. As l and σ decrease, azimuthal and inflow velocities become comparable. This is quite obvious from the vectors' direction (Figure 8c and d).

3.2.4. Effect of free parameters

It is time to discuss the properties and the physical implications that our achieved solutions involve. To conceive the role of free parameters on MHD behaviour of the disc, we plot the meridional dependency of the physical functions with respect to different values of these parameters. Incidentally, to have a better physical sense and direct interpretation, we plot them in physical units (SI), with the help of conversion factors calculated in Table 1.

Effect of electrical conductivity on some incompressible physical variables has been represented in Figure 9. Once conductivity grows large or resistivity becomes small, radial (Figure 9a) and meridional (Figure 9b) fluid velocities slow down. While, gas pressure (Figure 9c) and total density (Figure 9d) exceed, mass accretion rate (Figure 9e), rotational velocity, and magnetic pressure are not affected by resistivity at all. Magnetic pressure invariability and gas pressure ascent as σ goes up result in raising the ratio of gas to magnetic pressure β (Figure 9f).

Disc's rotation just influences the gas pressure, total density, and subsequently β (Figure 10). In other words, radial and meridional velocities as well as mass accretion rate (Figure 10c) and magnetic pressure are invariant relative to angular momentum parameter l . As disc rotates faster, gas pressure decreases (Figure 10a) and evidently via equation (50), disc becomes denser (Figure 10b). Obviously, it results in falling off β in this occasion (Figure 10d).

Although inflow velocity including radial and meridional components of fluid velocity is not impressed by rotation of the disc, they are affected by the spin of the central black hole. As central object spins faster, inflow velocity becomes faster (Figure 11a and b) and disc rotates faster too (Figure 11e). Gas pressure heightens (Figure 11c), while density falls off (Figure 11d). Descending behaviour of β (Figure 11f) indicates that the increase in magnetic pressure with accelerating the spin of the black hole is more than gas pressure.

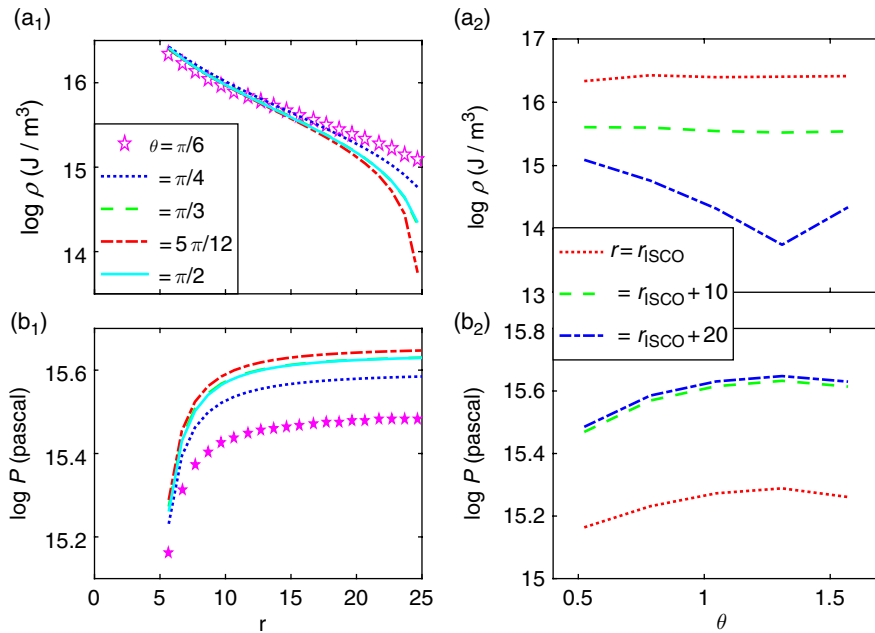


Figure 6. Repetition of the last two rows of Figure 5, but for $k = 1$.

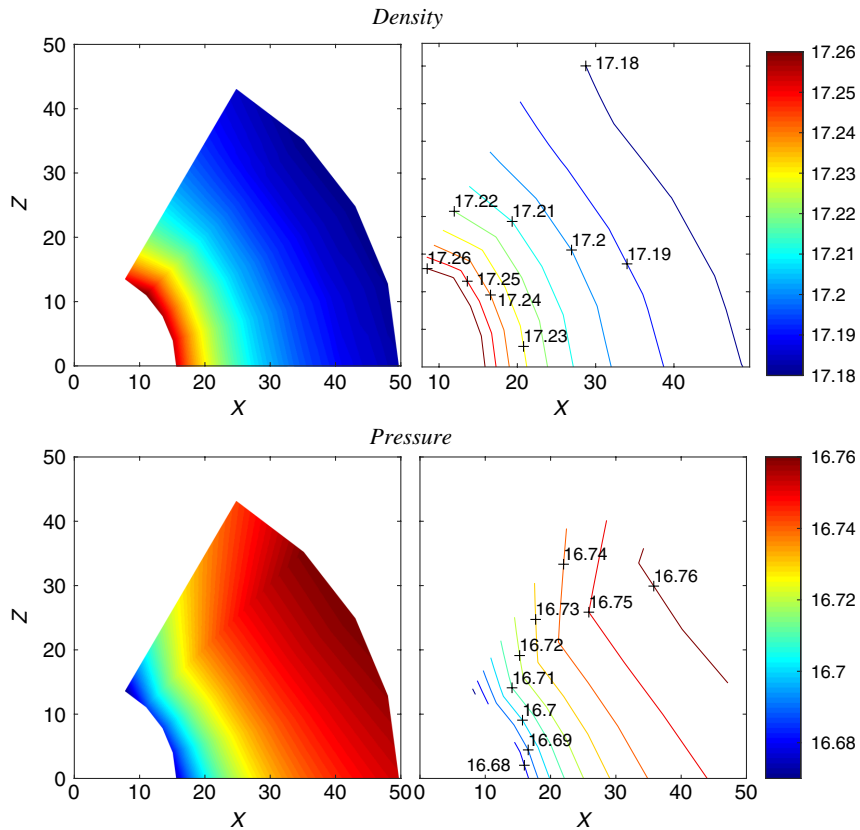


Figure 7. Density and pressure coloured distributions and contours in meridional plane. The constant parameters are the same as Figure 5.

In this interval, both C_1 has to be independent on r and total density must be positive. It means that if the profile of C_1 in a special radius does not coincident on that of C_1 in other radii also total

density is negative there, then that special radius must omit from our allowed radial interval. For the set $k = 1$, the inner edge of the disc rests on ISCO. However, for the other set ($k = 2$), disc starts

Table 1. Physical constants and conversion factors between code and SI units.

| Constant in SI units | Code value | | |
|---|-----------------------------|-----------------------|--|
| $G = 6.67384 \times 10^{-11} \text{ N.m}^2/\text{kg}^2$ | $G = 1$ | | |
| $M = 10 M_{\odot} = 20 \times 10^{30} \text{ kg}$ | $M = 1$ | | |
| $c = 3 \times 10^8 \text{ m/s}$ | $c = 1$ | | |
| $\mu = 1260 \times 10^{17} \text{ T.m}^3$ | $\mu = 5.2 \times 10^{-11}$ | | |
| Quantity | SI units | Geometric units | Conversion factor to SI units |
| Length | m | GMc^{-2} | $1.4831 \times 10^4 \text{ m}$ |
| Time | s | GMc^{-3} | $4.9436 \times 10^{-5} \text{ s}$ |
| Velocity | m/s | c | $3 \times 10^8 \text{ m/s}$ |
| Accretion rate | kg/s | $c^3 G^{-1}$ | $4.0456 \times 10^{35} \text{ kg/s}$ |
| Rest mass density | kg/m ³ | $c^6 G^{-3} M^{-2}$ | $6.1311 \times 10^{18} \text{ kg/m}^3$ |
| Internal energy per unit volume | J/m ³ | $c^8 G^{-3} M^{-2}$ | $5.5180 \times 10^{35} \text{ kg/(m.s}^2)$ |
| Pressure | pascal | $c^8 G^{-3} M^{-2}$ | $5.5180 \times 10^{35} \text{ kg/(m.s}^2)$ |
| Electrical conductivity | 1/s | $c^3 G^{-1} M^{-1}$ | $2.0228 \times 10^4 \text{ 1/s}$ |
| Magnetic field | T | $c^4 G^{-3/2} M^{-1}$ | $7.4283 \times 10^{17} \text{ T}$ |
| Magnetic dipole moment | T.m ³ | $G^{3/2} M^2 c^{-2}$ | $2.4232 \times 10^{30} \text{ T.m}^3$ |

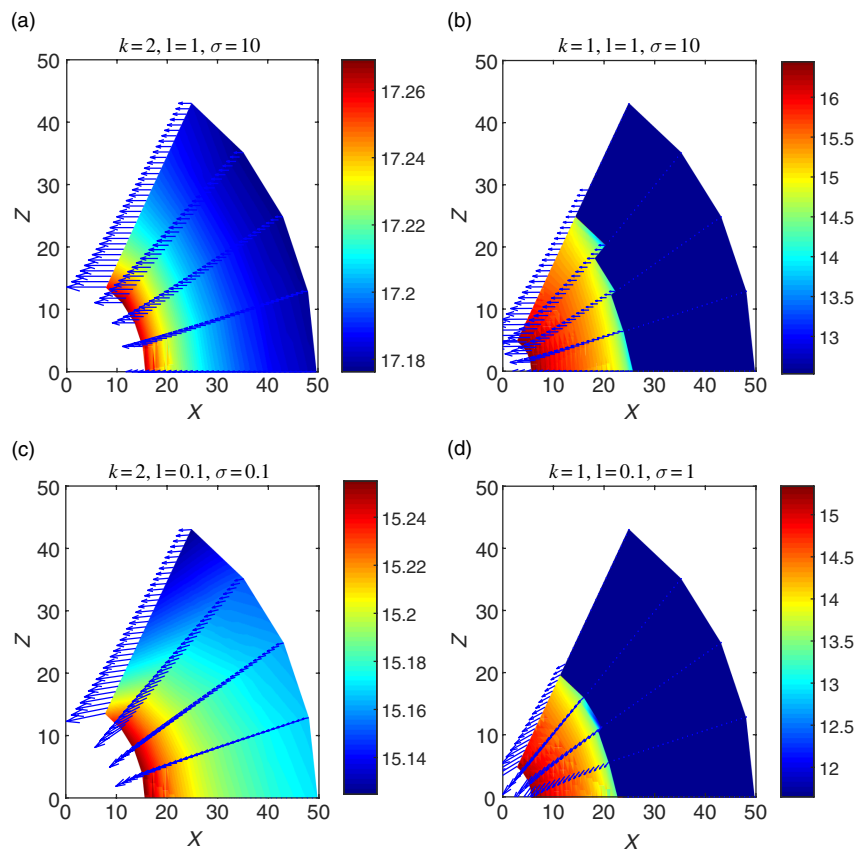


Figure 8. Density coloured distributions and meridional flow pattern for different values of k , l , and σ written in the title of each panel.

off 10 units farther than ISCO. Because next to ISCO, C_1 's profile seems to be dependent upon r (Figure 4). Besides the inner edge, these two sets of solutions about the outer edge have significant

discrepancy too. Occasionally, after a specific radius, it is possible that the total density becomes negative. It results in truncating the disc there. This is the event happened in the case of $k = 1$ and

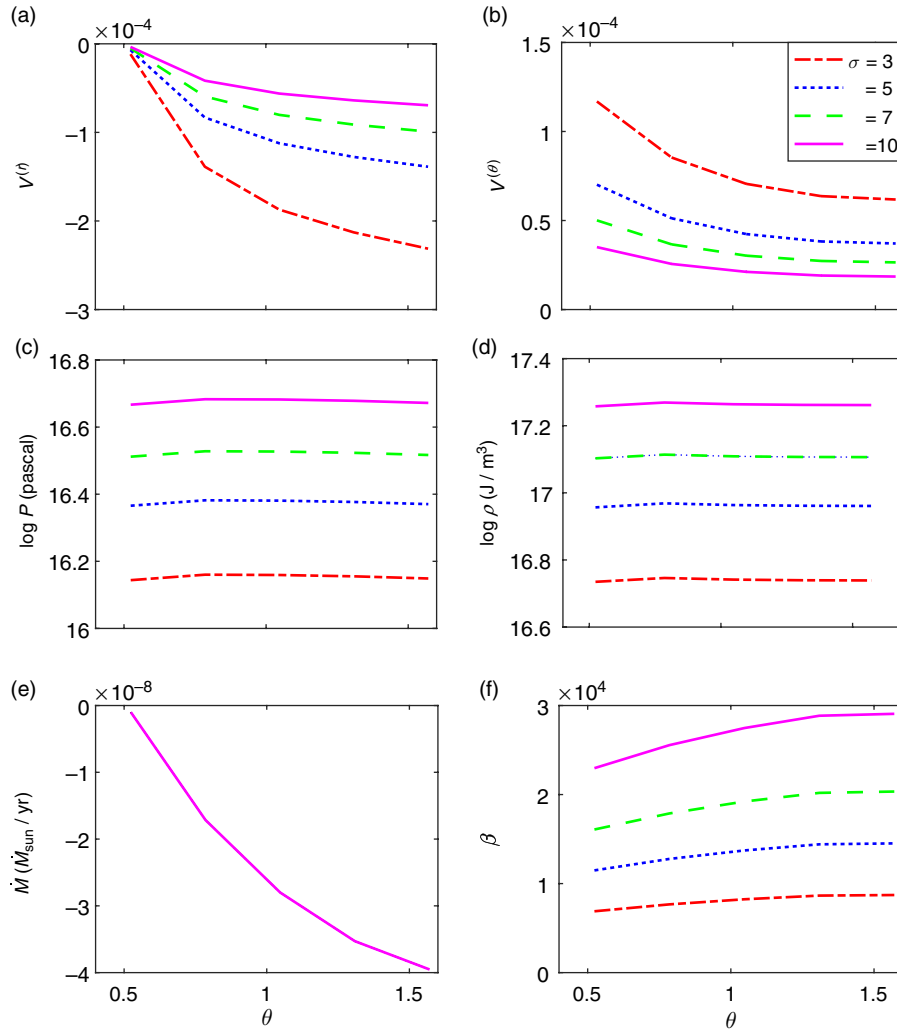


Figure 9. Meridional variation of (a) radial and (b) meridional velocities, (c) pressure (d) total density (e) mass accretion rate, and (f) ratio of the gas to magnetic pressure β , at radius r_{in} for different values of σ shown in the key. The other constant parameters are $a = 0.1$, $l = 1$, $k = 2$, and $\dot{M}_0 = -10^{-8} \frac{M_{\odot}}{\text{year}}$.

restricts the disc's outer radius. That is why the disc in this case is radially shorter than the other case (Figure 6a₁ and b₁).

Larger the value of mass accretion rate constant \dot{M}_0 (Figure 12c), higher are the values of gas pressure (Figure 12a), total density (Figure 12b), and the ratio of gas to magnetic pressure β (Figure 12d).

k ascent leads to decelerate the radial (Figure 13a) and vertical (Figure 13b) inflow velocities and heightening the gas pressure (Figure 13c), total density (Figure 13d), and mass accretion rate (Figure 13e). In addition, it results in sharp variations in β around the equator (Figure 13f).

4. Discussion and conclusion

Analytical and numerical (semi-analytical) investigations of thick accretion discs around a rotating compact object in presence of an external dipolar magnetic field considering all three components of the fluid velocity have not been carried out in any detail so far. In this paper, we have developed an axisymmetric stationary two-dimensional model of the magnetised tori accreted from the resistive plasma surrounding a rotating black hole. Importance of

the general relativity in the discussions of accretion physics around a black hole is no secret to anyone and the full relativistic treatment is required. Consequently, we have derived the governing MHD equations in the full general relativistic framework. They are a coupled set of highly non-linear equations that are in general so difficult to solve. To avoid the mathematical complexities, we employ the linear order approximation on the Kerr parameter a and ignore the effects of radiation field.

These simplifying assumptions are indeed considered as practical approximations applicable to the full general relativistic MHD system. Additionally, assumption of similar radial dependency for the radial and meridional velocities resulting in a simple form for mass accretion rate helps a lot in solving the equations.

Moreover, considering a special model for the toroidal magnetic field leads to the fact that the radial and meridional components of the 4-vector current density are vanished. The azimuthal current produced owing to the motion of the magnetofluid generates a poloidal magnetic field inside the disc as well. It has been depicted that the disc's poloidal magnetic field and the spin of the central black hole are strongly related. Connection of the disc field to the external dipolar field occurs due to the presence of

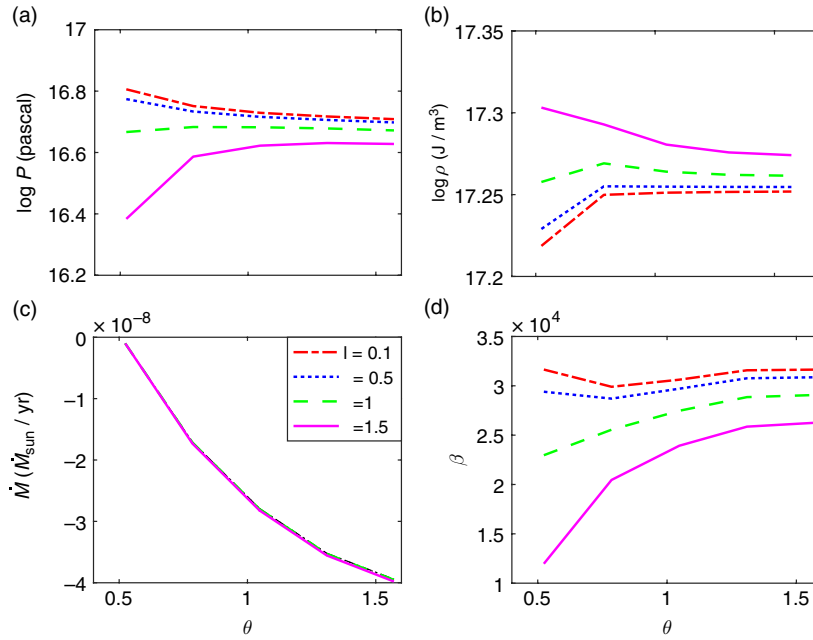


Figure 10. Meridional variation of (a) pressure, (b) total density, (c) mass accretion rate, and (d) ratio of the gas to magnetic pressure β , at radius r_m for different values of l shown in the key. The other constant parameters are $a = 0.1$, $\sigma = 10$, $k = 2$, and $\dot{M}_0 = -10^{-8} \frac{M_{\odot}}{\text{year}}$.

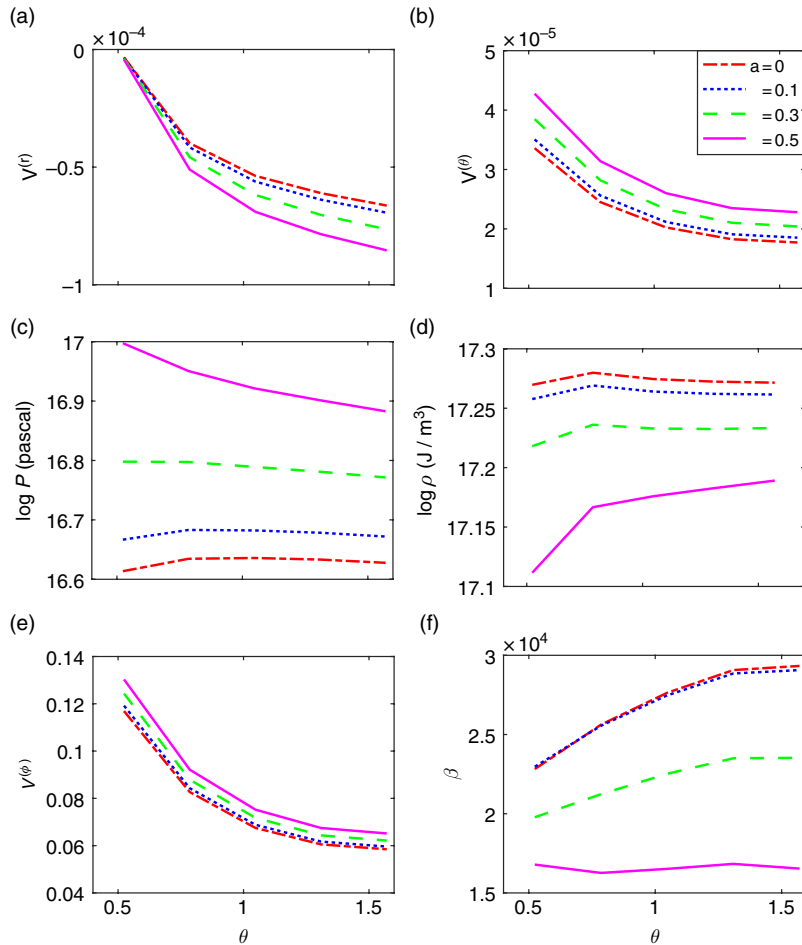


Figure 11. Meridional variation of (a) radial and (b) meridional velocities, (c) pressure, (d) total density, (e) azimuthal velocity, and (f) ratio of the gas to magnetic pressure β , at radius r_m for different values of a shown in the key. The other constant parameters are $l = 1$, $k = 2$, $\sigma = 10$, and $\dot{M}_0 = -10^{-8} \frac{M_{\odot}}{\text{year}}$.

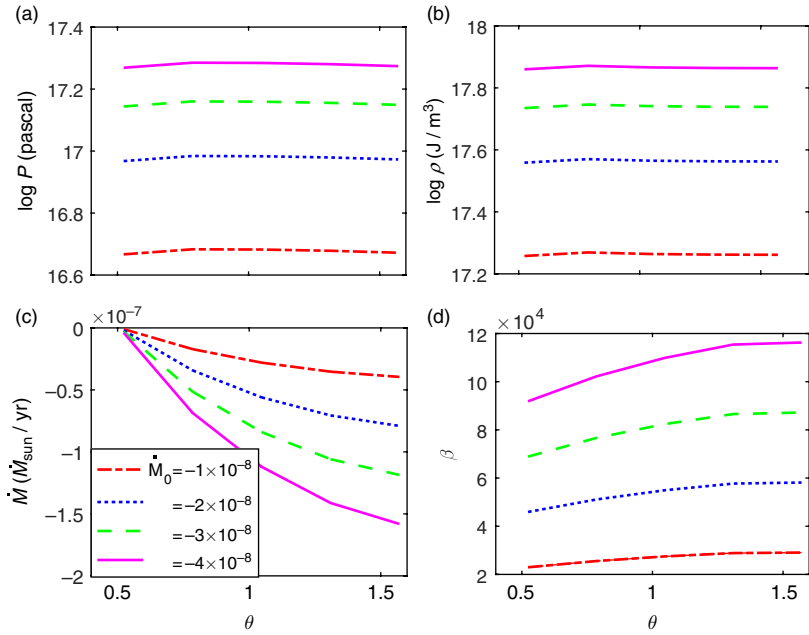


Figure 12. Meridional variation of (a) pressure, (b) total density, (c) mass accretion rate, and (d) ratio of the gas to magnetic pressure β , at radius r_m for different values of \dot{M}_0 shown in the key. The other constant parameters are $a = 0.1$, $l = 1$, $\sigma = 10$, and $k = 2$.

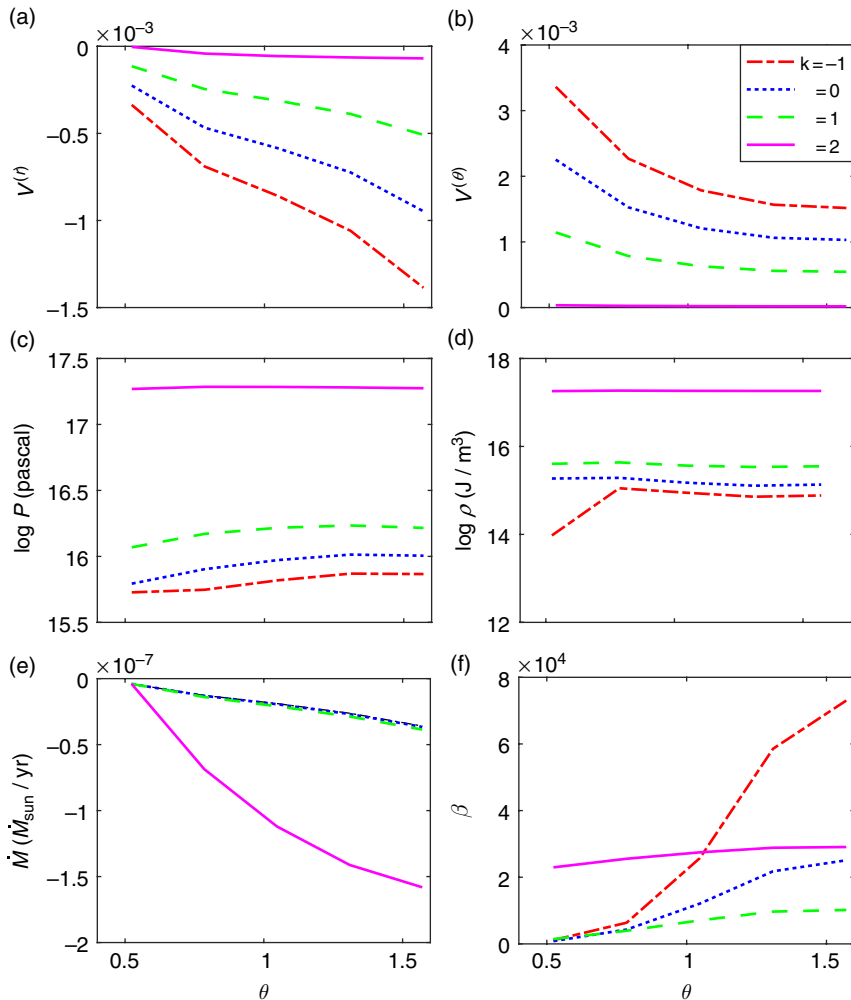


Figure 13. Meridional variation of (a) radial and (b) meridional velocities, (c) pressure, (d) total density, (e) mass accretion rate, and (f) ratio of the gas to magnetic pressure β , at radius r_{in} for different values of k shown in the key. The other constant parameters are $l = 1$, $a = 0.1$, $\sigma = 10$, and $\dot{M}_0 = -10^{-8} \frac{M_{\odot}}{\text{year}}$.

the finite conductivity for the plasma. The meridional structure of the disc is mainly on account of the balance of plasma pressure gradient, magnetic force due to the poloidal magnetic field, and the centrifugal force. In our scenario, different free parameters are determinant and play a crucial role in calculating the accretion tori features and have a major influence on process of accretion around a black hole.

In conclusion, we find that the self-consistent equilibrium solutions in the relativistic framework do exist for a slowly rotating black hole with a dipolar magnetic field accreting matter from a disc having all the components of velocity non-zero without invoking any thin disc approximations. The existence of such an equilibrium structure encourages one to put aside our simplifying assumptions gradually and look for generalisations of the analysis to a rapidly rotating central black hole. On the other hand, yet another important aspect to be considered is the generalisation of the analysis to cases where a toroidal magnetic field is generated by the inertia of the plasma and backward bending the external dipolar magnetic field lines. This toroidal magnetic field is associated with a hoop stress that can collimate a hydromagnetic outflow over large distances and form a jet.

This work can also be useful for the general relativistic MHD simulations that suffer mainly from the lack of exact analytical and semi-analytical solutions to use as initial conditions and to compare their achieved results.

References

Abramowicz, M. A., Karas, V., & Lanza, A. 1998, *A&A*, 331, 1143
 Banerjee, D., Bhatt, J. R., Das, A. C., & Prasanna, A. R. 1995, *ApJ*, 449, 789
 Banerjee, D., Bhatt, J. R., Das, A. C., & Prasanna, A. R. 1997, *ApJ*, 474, 389
 Bardeen, J. M., Press, W. H., & Teukolsky, S. A. 1972, *ApJ*, 178, 347
 De Villiers, J.-P., Hawley, J. F., & Krolik, J. H. 2003, *ApJ*, 599, 1238
 Eyink, G., & Aluie, H. 2006, *Physica D*, 223, 82
 Fleming, T. P., & Stone, J. M. 2003, *ApJ*, 585, 908
 Font, J. A., & Daigne, F. 2002, *MNRAS*, 334, 383
 Foucart, F., Chandra, M., Gammie, C. F., & Quataert, E. 2016, *MNRAS*, 456, 1332
 Foucart, F., Chandra, M., Gammie, C. F., Quataert, E., & Tchekhovskoy, A. 2017, *MNRAS*, 470, 2240
 Gammie, C. F., & McKinney, J. 2003, *ApJ*, 589, 444
 Gammie, C. F., & Menou, K. 1998, *ApJ*, 332, 659
 Ghosh, P. 2000, *MNRAS*, 315, 89
 Ghosh, P., & Lamb, F. K. 1979a, *ApJ*, 232, 259
 Ghosh, P., & Lamb, F. K. 1979b, *ApJ*, 234, 296
 Harko, T., Kovacs, Z., & Lobo, F. S. N. 2011, *CQGra*, 28, 165001
 Higginbottom, N., Knigge, C., Long, K. S., Matthews, J. H., Sim, S. A., & Hewitt, H. A. 2018, *MNRAS*, 479, 3651
 Kaburaki, O. 1986, *MNRAS*, 220, 321
 Kaburaki, O. 1987, *MNRAS*, 229, 165
 Kudoh, T., & Kaburaki, O. 1996, *ApJ*, 460, 199
 Koide, S. 2010, *ApJ*, 708, 1459
 Koide, S., Shibata, K., & Kudoh, T. 1999, *ApJ*, 522, 727
 Kovar, J., Slany, P., Stuchlik, Z., Karas, V., Cremaschini, C., & Miller, J. C. 2011, *PhRvD*, 84, 4002
 Lee, W.H. & Ruiz, E.R. 2002, *ApJ*, 577, 893
 Li, L.-X. 2000, *PhRvD*, 61, 084016
 McKinney, J. C., & Gammie, C. F. 2004, *ApJ*, 611, 977
 Okuda, T. 2002, *PASJ*, 54, 253
 Porth, O. 2019, *ApJS*, 243, 26
 Prasanna, A. R. 1989, *A&A*, 217, 329
 Prasanna, A. R., & Vishveshwara C. V. 1978, *Pramana*, 11, 359
 Rezzolla, L., Ahmedov, B. J., & Miller, J. C. 2001, *MNRAS*, 322, 723
 Robertson, S. L., & Leiter, D. J. 2002, *ApJ*, 565, 447

Shakura, N. I., & Sunyaev, R. A. 1973, *A&A*, 24, 337
 Shaghaghian, M. 2011, *MNRAS*, 415, 534
 Shaghaghian, M. 2016, *MNRAS*, 456, 1528
 Takahashi, H. R., & Ohsuga, K. 2015, *PASJ*, 67, 60
 Takahashi, M., & Koyama, H. 2009, *ApJ*, 693, 472
 Takeuchi, S., Ohsuga, K., & Mineshige, S. 2010, *PASJ*, 62, L43
 Tchekhovskoy, A., Narayan, R., & McKinney, J. C. 2011, *MNRAS*, 418, L79
 Tomimatsu, A., & Takahashi, M. 2001, *ApJ*, 552, 710
 Tripathy, S. C., Prasanna, A. R., & Das, A. C. 1990, *MNRAS*, 246, 384
 Trova, A., Schroven, K., Hackmann, E., Karas, V., Kovar, J., & Slany, P. 2018, *PhRvD*, 97, 4019
 Yokosawa, M., & Inui, T. 2005, *ApJ*, 631, 1051
 Yuan, F., & Narayan, R. 2014, *ARA&A*, 52, 529

Appendix A

A.1. Magnetic field lines

Magnetic field lines are curved lines drawn in space in such a way that a tangent line at any point is parallel to the magnetic field vector at that point. Slope of this line in any point (r, θ) , in spherical coordinate, is defined by $\frac{dr}{r d\theta}$. On the other hand, slope of the magnetic field in that point is defined by $\frac{B_{(r)}}{B_{(\theta)}}$. Thus, we have

$$\frac{dr}{r d\theta} = \frac{B_{(r)}}{B_{(\theta)}}. \quad (A1)$$

It gives

$$-2 \cot \theta d\theta = \frac{dr}{r}, \quad (A2)$$

for poloidal magnetic field of the central black hole in the limit $(\frac{m}{r} \ll 1)$, and gives

$$- \cot \theta d\theta = \left[\frac{1}{r} + \frac{\frac{6 a L}{r^4}}{1 - \frac{2 a L}{r^3}} \right] dr, \quad (A3)$$

for the disc. On account of the linearised approximation on a , it is good to notify that the terms including a^2 have been ignored. Integrating the differential equation (A2), it yields

$$r = \frac{r_0}{\sin^2 \theta},$$

for the seed field. Do the same work for equation (A3), it provides an algebraic equation

$$r^2 \left(r - \frac{r_0}{\sin \theta} \right) = 2 a L.$$

Solving it, we have

$$r = \frac{1}{6} Q + \frac{2}{3} \frac{d^2}{Q} + \frac{1}{3} d,$$

for the disc field. Where

$$Q = \left(108 b + 8 d^3 + 12 \sqrt{12 d^3 b + 81 b^2} \right)^{1/3}, \quad (A4)$$

$$d = \frac{r_0}{\sin \theta}, \quad (A5)$$

$$b = 2 a L, \quad (A6)$$

and r_0 is a constant of integration. Considering the toroidal magnetic field and knowing the relation

$$\frac{dr}{B_{(r)}} = \frac{r d\theta}{B_{(\theta)}} = \frac{r \sin \theta d\varphi}{B_{(\varphi)}},$$

between the components of the magnetic field, we achieve

$$\varphi = \varphi_0 + \frac{b_\varphi}{B_1} \frac{1}{k-1} \frac{r^{1-k}}{\sin^k \theta \cos \theta}.$$

To visualise the field line structure, it is usual to transform to a Cartesian frame through the relations $X = r \sin \theta \cos \varphi$, $Y = r \sin \theta \sin \varphi$, and $Z = r \cos \theta$.

Appendix B

B.1. Derivation of $\Psi(r, \theta)$

At first, rewrite equation (35) as

$$(\rho + p) (1 - V^2)^{-1} = \frac{\dot{M}_0 C_1(\theta)}{r^2 \sin \theta V^{(r)} \left(1 - \frac{2}{r}\right) \left(1 - \frac{2aL}{r^3}\right)^{-1}},$$

and substitute it in momentum equations (24) and (25), to achieve the components of pressure gradient

$$\begin{aligned} \frac{\partial p}{\partial r} &= \frac{-\dot{M}_0}{\left(1 - \frac{2}{r}\right) \left(1 - \frac{2aL}{r^3}\right)^{-1} r^2 \sin \theta} N_1(r, \theta) \\ &+ \left(1 - \frac{2}{r}\right)^{-1/2} J^{(\varphi)} [B_{(\theta)} \{1 - [V^{(\varphi)}]^2\} + B_{(\varphi)} V^{(\theta)} V^{(\varphi)}], \end{aligned} \tag{B1}$$

$$\begin{aligned} \frac{\partial p}{\partial \theta} &= \frac{-\dot{M}_0 C_1(\theta)}{\sin \theta} \left\{ \frac{1}{r} \left(1 - \frac{2aL}{r^3}\right) N_3(r, \theta) \right. \\ &+ \frac{6aL}{r^5} \tilde{V}^{(\theta)} - \frac{L^2}{r^4 \sin^2 \theta} \left(1 - \frac{2aL}{r^3}\right)^{-1} \frac{\cot \theta}{C_1(\theta) \tilde{V}^{(\theta)}} \left. \right\} \\ &- r J^{(\varphi)} [B_{(r)} \{1 - [V^{(\varphi)}]^2\} + B_{(\varphi)} V^{(r)} V^{(\varphi)}]. \end{aligned} \tag{B2}$$

Then, calculate the pressure second derivatives

$$\begin{aligned} \frac{\partial^2 p}{\partial \theta \partial r} &= \frac{-\dot{M}_0}{\left(1 - \frac{2}{r}\right) \left(1 - \frac{2aL}{r^3}\right)^{-1} r^2 \sin \theta} \\ &\left\{ -\cot \theta N_1(r, \theta) + \frac{\partial N_1(r, \theta)}{\partial \theta} \right\} + N_2(r, \theta), \end{aligned} \tag{B3}$$

$$\begin{aligned} \frac{\partial^2 p}{\partial r \partial \theta} &= \frac{-\dot{M}_0 C_1(\theta)}{\sin \theta} \left\{ N_3(r, \theta) \left(\frac{-1}{r^2} + \frac{8aL}{r^5} \right) \right. \\ &+ \frac{1}{r} \left(1 - \frac{2aL}{r^3}\right) \frac{\partial N_3(r, \theta)}{\partial r} - \frac{30aL}{r^6} \tilde{V}^{(\theta)} + \frac{6aL}{r^5} \frac{\partial \tilde{V}^{(\theta)}}{\partial r} \\ &+ \frac{L^2}{r^4 \sin^2 \theta} \left(1 - \frac{2aL}{r^3}\right)^{-1} \frac{\cot \theta}{C_1(\theta) \tilde{V}^{(\theta)}} \\ &\left. \left[\left(4 - \frac{2aL}{r^3}\right) \frac{1}{r} \left(1 - \frac{2aL}{r^3}\right)^{-1} + \frac{1}{\tilde{V}^{(\theta)}} \frac{\partial \tilde{V}^{(\theta)}}{\partial r} \right] \right\} \\ &- \left[B_{(r)} J^{(\varphi)} + r \frac{\partial B_{(r)}}{\partial r} J^{(\varphi)} + r B_{(r)} \frac{\partial J^{(\varphi)}}{\partial r} \right] \{1 - [V^{(\varphi)}]^2\} \\ &+ 2 V^{(\varphi)} \frac{\partial V^{(\varphi)}}{\partial r} r B_{(r)} J^{(\varphi)} \\ &- \left[J^{(\varphi)} B_{(\varphi)} + r \frac{\partial J^{(\varphi)}}{\partial r} B_{(\varphi)} + r J^{(\varphi)} \frac{\partial B_{(\varphi)}}{\partial r} \right] V^{(r)} V^{(\varphi)} \\ &- \left[\frac{\partial V^{(r)}}{\partial r} V^{(\varphi)} + V^{(r)} \frac{\partial V^{(\varphi)}}{\partial r} \right] r J^{(\varphi)} B_{(\varphi)}, \end{aligned} \tag{B4}$$

where

$$\begin{aligned} N_1(r, \theta) &= [C_1(\theta)]^2 \frac{\partial \tilde{V}^{(\theta)}}{\partial r} + \frac{1}{r} C_1(\theta) \frac{\partial \tilde{V}^{(\theta)}}{\partial \theta} + \frac{1}{r} \tilde{V}^{(\theta)} \frac{dC_1(\theta)}{d\theta} \\ &- \frac{1}{r} \left[\left(1 - \frac{2}{r}\right) \tilde{V}^{(\theta)} + \frac{[V^{(\varphi)}]^2}{\tilde{V}^{(\theta)}} \right] \\ &+ \left[\frac{1}{r^2} \left(1 - \frac{2}{r}\right)^{-1} - \frac{6aL}{r^4} \left(1 - \frac{2aL}{r^3}\right)^{-1} \right] \\ &\times \left[\frac{1}{\tilde{V}^{(\theta)}} - [C_1(\theta)]^2 \tilde{V}^{(\theta)} \right], \\ \frac{\partial N_1(r, \theta)}{\partial \theta} &= 2 \frac{dC_1(\theta)}{d\theta} \left[C_1(\theta) \frac{\partial \tilde{V}^{(\theta)}}{\partial r} + \frac{1}{r} \frac{\partial \tilde{V}^{(\theta)}}{\partial \theta} \right] \\ &+ [C_1(\theta)]^2 \frac{\partial^2 \tilde{V}^{(\theta)}}{\partial \theta \partial r} + \frac{1}{r} C_1(\theta) \frac{\partial^2 \tilde{V}^{(\theta)}}{\partial \theta^2} + \frac{1}{r} \tilde{V}^{(\theta)} \frac{d^2 C_1(\theta)}{d\theta^2} \\ &- \frac{1}{r} \left(1 - \frac{2}{r}\right) \frac{\partial \tilde{V}^{(\theta)}}{\partial \theta} - \frac{2}{r} \frac{V^{(\varphi)}}{\tilde{V}^{(\theta)}} \frac{\partial V^{(\varphi)}}{\partial \theta} + \frac{1}{r} \left[\frac{V^{(\varphi)}}{\tilde{V}^{(\theta)}} \right]^2 \frac{\partial \tilde{V}^{(\theta)}}{\partial \theta} \\ &- \left[\frac{1}{r^2} \left(1 - \frac{2}{r}\right)^{-1} - \frac{6aL}{r^4} \left(1 - \frac{2aL}{r^3}\right)^{-1} \right] \\ &\left[\left\{ \frac{1}{[\tilde{V}^{(\theta)}]^2} + [C_1(\theta)]^2 \right\} \frac{\partial \tilde{V}^{(\theta)}}{\partial \theta} - 2 C_1(\theta) \tilde{V}^{(\theta)} \frac{dC_1(\theta)}{d\theta} \right], \\ N_2(r, \theta) &= \left(1 - \frac{2}{r}\right)^{-1/2} \left\{ \left[\frac{\partial B_{(\theta)}}{\partial \theta} J^{(\varphi)} + B_{(\theta)} \frac{\partial J^{(\varphi)}}{\partial \theta} \right] \{1 - [V^{(\varphi)}]^2\} \right. \\ &\left. - 2 V^{(\varphi)} \frac{\partial V^{(\varphi)}}{\partial \theta} B_{(\theta)} J^{(\varphi)} \right\} \end{aligned}$$

$$\begin{aligned}
 & + \left[\frac{\partial J^{(\varphi)}}{\partial \theta} B_{(\varphi)} + J^{(\varphi)} \frac{\partial B_{(\varphi)}}{\partial \theta} \right] \tilde{V}^{(\theta)} V^{(\varphi)} \\
 & + \left[\frac{\partial V^{(\theta)}}{\partial \theta} V^{(\varphi)} + \tilde{V}^{(\theta)} \frac{\partial V^{(\varphi)}}{\partial \theta} \right] J^{(\varphi)} B_{(\varphi)}, \\
 N_3(r, \theta) & = \frac{\partial \tilde{V}^{(\theta)}}{\partial r} + \frac{1}{r^2} \left(1 - \frac{2}{r}\right)^{-1/2} \tilde{V}^{(\theta)} \\
 & + \frac{1}{r C_1(\theta)} \frac{\partial \tilde{V}^{(\theta)}}{\partial \theta} + \left(1 - \frac{3}{r}\right) \left(1 - \frac{2}{r}\right)^{-1} \frac{\tilde{V}^{(\theta)}}{r}, \\
 \frac{\partial N_3(r, \theta)}{\partial r} & = \frac{\partial^2 \tilde{V}^{(\theta)}}{\partial r^2} + \frac{\tilde{V}^{(\theta)}}{r^2} \left(1 - \frac{2}{r}\right)^{-2} \left[-1 + \frac{6}{r} \left(1 - \frac{1}{r}\right) \right. \\
 & \left. + \frac{1}{r} \left(1 - \frac{2}{r}\right)^{1/2} \left(-2 + \frac{3}{r}\right) \right] \\
 & + \frac{1}{r C_1(\theta)} \left(-\frac{1}{r} \frac{\partial \tilde{V}^{(\theta)}}{\partial \theta} + \frac{\partial^2 \tilde{V}^{(\theta)}}{\partial r \partial \theta} \right) \\
 & + \frac{1}{r} \left(1 - \frac{2}{r}\right)^{-1} \frac{\partial \tilde{V}^{(\theta)}}{\partial r} \left[\frac{1}{r} \left(1 - \frac{2}{r}\right)^{1/2} + \left(1 - \frac{3}{r}\right) \right].
 \end{aligned}$$

Integrability condition for pressure

$$\frac{\partial^2 p}{\partial \theta \partial r} = \frac{\partial^2 p}{\partial r \partial \theta}, \tag{B5}$$

gives a second-order ordinary differential equation for $C_1(\theta)$. In order to ready this differential equation for computer code to solve it numerically, we arrange it in the form

$$\frac{d^2 C_1(\theta)}{d\theta^2} = \Psi(r, \theta).$$

It means that we must sort the differential equation (B5) in terms of $\frac{d^2 C_1(\theta)}{d\theta^2}$. This term, not only appears in the fifth term in $\frac{\partial N_1(r, \theta)}{\partial \theta}$ clearly, but also $\frac{\partial^2 \tilde{V}^{(\theta)}}{\partial \theta^2}$ includes it. Thus, equation (B5) may be rewritten as

$$\begin{aligned}
 & \frac{-\dot{M}_0}{\left(1 - \frac{2}{r}\right) \left(1 - \frac{2aL}{r^3}\right)^{-1} r^2 \sin \theta} \left\{ N_4(r, \theta) \right. \\
 & \left. + \frac{1}{r} \left[\psi(r, \theta) C_1(\theta) + \tilde{V}^{(\theta)} \right] \frac{d^2 C_1(\theta)}{d\theta^2} \right\} + N_2(r, \theta) = \frac{\partial^2 p}{\partial r \partial \theta},
 \end{aligned}$$

wherein $N_4(r, \theta) = -\cot \theta N_1(r, \theta) +$ all the terms of $\frac{\partial N_1(r, \theta)}{\partial \theta}$ exclude the terms including $\frac{d^2 C_1(\theta)}{d\theta^2}$. Thus,

$$\Psi(r, \theta) = \frac{-\frac{r^2 \sin \theta}{M_0} \left(1 - \frac{2}{r}\right) \left(1 - \frac{2aL}{r^3}\right)^{-1} \left[\frac{\partial^2 p}{\partial r \partial \theta} - N_2(r, \theta) \right] - N_4(r, \theta)}{\frac{1}{r} \left[\psi(r, \theta) C_1(\theta) + \tilde{V}^{(\theta)} \right]},$$

here

$$\begin{aligned}
 \psi(r, \theta) & = -\frac{S_0}{2} \frac{YI^{3/2}}{1 - [V^{(\varphi)}]^2} \left[2 S_1 A_1 r \left(1 - \frac{2}{r}\right)^{-1/2} \right. \\
 & \left. + 2 (S_0 Y)^2 C_1(\theta) \right].
 \end{aligned}$$